Clustering in structure and reactions using configuration interaction techniques

Konstantinos Kravvaris* and Alexander Volya
Department of Physics, Florida State University, Tallahassee, Florida 32306, USA

(Received 18 September 2018; revised manuscript received 27 May 2019; published 23 September 2019)

Background: Atomic nuclei are remarkable quantum many-body systems where clustering properties develop naturally from underlying interactions between the constituent nucleons. Clustering degrees of freedom manifest themselves in multiple structure and reaction observables.
Purpose: Our goal is to study nuclear clustering and its emergence in many-nucleon dynamics from nucleon-nucleon interactions. Clustering is a phenomenon that is known to emerge on the boundary between structure and reactions, therefore developing appropriate techniques that bridge the structure-reaction divide and establishing connections to observables is among our principal objectives. Showing consistency and how the new techniques can be reduced to well established other methods is an important part of this work.
Methods: The configuration-interaction technique based on second quantization is used to treat the quantum many-body problem assuring that fermionic antisymmetry is fully satisfied. The use of the harmonic oscillator single-particle basis allows for the center-of-mass coordinate to be separated and prepared in a desired oscillator state for each cluster. The relative motion reaction basis channels are constructed by coupling clusters in different harmonic oscillator states with respect to their relative motion. Finally, using a resonating group method strategy we solve the generalized eigenvalue problem to obtain scattering channels. Structural clustering characteristics are discussed and the modified harmonic oscillator representation for scattering equations method is used to extract scattering observables.
Results: New methods for treating clustering problems have been put forward. We demonstrate broad applicability of the developed techniques. Examples highlight connections with algebraic techniques, and the role of approximations leading to algebraic limits is assessed using realistic examples. Various types of clustering characteristics are used to study alpha clustering in light nuclei that are relevant to currently ongoing experimental efforts. We demonstrate the emergence of strongly clustered bands of states in beryllium, triple alpha channels in ^{12}C, and molecular type clustering in ^{21}Ne. Starting from nucleon-nucleon interactions without any additional assumptions scattering phase shifts for alpha-alpha scattering are determined and shown to be consistent with those observed.
Conclusions: In this work we put forward a new configuration-interaction-based method that targets the physics of clustering, and further unifies nuclear structure and reactions. We provide detailed discussions and many examples highlighting features and advantages of the approach.

DOI: 10.1103/PhysRevC.100.034321

I. INTRODUCTION

Understanding the formation of substructures within atomic nuclei, also known as nuclear clustering, from microscopic principles remains one of the most complex problems in nuclear physics. This emergence of clustering from the nucleon-nucleon interactions has a significant impact on the structure of light nuclei. Along with clustering, the emergence of regularities such as nuclear shell structure, rotational bands, and vibrational states to name a few, and their interplay, is a central question of modern nuclear many-body physics [1,2].

In the following part of this Introduction we highlight several key theoretical questions addressed in this work along with some abbreviated historical perspectives that help to position our work in the field.

The concept of a nucleus as being comprised of α particles has existed since the early days of nuclear physics [3–5]. Strong binding of an α particle and abundance of experimentally known α decaying elements support this concept. In further support, theories in Refs. [3,4,6] emphasized that the binding energies of $N = Z$ nuclei seem to be proportional to the number of bonds that can be made between the α constituents of the nucleus. Currently, the antisymmetrized molecular dynamics method continues this direction of work, being extensively applied to the problem of molecular-type states in clustered nuclei [7]. Such states are known to exist in $N > Z$ nuclei [8,9], with the extra neutrons forming valence bonds between the α, or other heavier cores, similar to the role of electrons in molecules. Relying on group theory, algebraic symmetry-based approaches have been used to further explore molecularlike physics of clustering suggesting triangular and tetrahedral spatial symmetries in ^{12}C and ^{16}O [10,11].

*Present address: Lawrence Livermore National Laboratory, P. O. Box 808, Livermore, CA 94551, USA.

With the discovery of the neutron, attention shifted to models built using nucleonic degrees of freedom, such as the nuclear shell model. Cluster models and the nuclear shell model have been evolving in parallel, presenting a need for a unified theory that would explain the emergence and survival of clustering.

A vast number of states possessing cluster characteristics of both α and non-α type [12,13] were found to lie at energies near the respective cluster decay threshold, prompting Ikeda to exemplify this property in the, now famous, Ikeda diagram [14]. This idea ties in nicely with the Gamow theory of α decay, in which an already preformed α particle tunnels from the nuclear surface through the Coulomb barrier. Our theoretical interest today targets the question of quantum many-body structure and its interaction with reaction continuum. Clustered states and clustered rotational bands in many nuclei, including those with $N = Z$, have been observed with high angular momentum, deeply in the continuum at very high excitation energies, and remarkably unmixed with enormous number of other states [15–17]. The role of coupling to the reaction continuum in reorganizing quantum many-body structure into a few superradiant states that are strongly coupled and separating them from those that nearly do not decay has been actively discussed recently [18–21].

The triple-α clustered, second excited 0^+ state in ^{12}C is among the most important ones in astrophysics. In 1954 Sir Fred Hoyle predicted [22,23] the existence of this state as a necessary doorway for the creation of ^{12}C in the universe. Given that the 2α system ^{8}Be is unbound, and there exists no bound $A = 5$ system, the formation of elements heavier than $A = 4$ would otherwise be hindered. From this argument the state is expected to have a strong triple-α character, a result verified experimentally. Only recently it has been shown that the decay proceeds predominantly through the short-lived ^{8}Be 0^+ ground state resonance [24–28]. Complex multifragment decay channels, internal structure and final state interactions are all challenging theoretical questions; see Ref. [29] and references therein.

In the 1970s a large body of experimental data was collected aiming at investigating cluster aspects of light nuclei; see Refs. [30–32] for some specific examples, or Ref. [33] for a more complete survey of experimental data. The main tools of choice were the α transfer reactions, such as $(^6\mathrm{Li}, d)$, $(^7\mathrm{Li}, t)$, and α knockout reactions such as $(p, p\alpha)$. These reactions were found to be selective to populating or depopulating states with some degree of clusterization. Attempts to describe α clustering using the many-body techniques of the nuclear shell model led to the development of powerful SU(3) symmetry-based approaches [34,35]. Despite some degree of success [36,37], significant deviations from experiment call for further theoretical research. This is one of the motivating factors for this work.

Coupling of the many-body structure to cluster reactions gave rise to the resonating group method (RGM) [38,39], which aimed at an explicit description of the nucleus as a multifragment clustered state, while maintaining a microscopic description for the cluster fragments and employing a fully antisymmetric wave function on the nucleonic level. The method based on harmonic oscillator representation of scattering equations (HORSE) [40] has been widely used recently to tackle the structure-reactions interface.

Using Green's function Monte Carlo calculations the emergence of clustering in ^{8}Be has been demonstrated starting from a nucleon-nucleon (NN) interaction [41]. This fundamental result reignited present-day theoretical interest to clustering; mean field approaches [42], lattice models [43,44], large-scale *ab initio* shell model calculations [45], and Bose-Einstein condensate wave functions [46–48] have all been employed in an attempt to better understand how the clusters are formed, and which aspects of nuclear structure and reactions are most affected by the formation of substructures within the nucleus.

In this work we seek to further advance and bring closer the above-mentioned questions and research directions.

We describe clustering starting with nucleon degrees of freedom and nucleon-nucleon interactions, and show the emergence of clustering degrees of freedom without any *a priori* assumptions. We make an explicit effort to connect our work with algebraic techniques which highlight the transitional physics between the single particle and collective pictures of the nucleus. Finally, we bridge structure and reaction physics and discuss the connection between theoretical clustering characteristics and experimentally extracted quantities such as spectroscopic factors and scattering phase shifts.

The work is organized as follows. In Sec. II we present theory concerning the many-body structure of clustering channels; this includes a review of the configuration interaction technique, treatment of the center of mass in the harmonic oscillator (HO) basis and manipulations using the boosting technique, construction of special many body configurations that correspond to clustered states (referred to in our work as cluster basis channels), and finally we use these cluster basis states as a basis for the RGM approach where the many-body Hamiltonian is used to determine the resonant cluster channel variationally.

In Sec. II we also highlight the important connections of this theory with previously used methods. We show that basis cluster channels take the form of stretched irreducible representations of SU(3) algebra if some simplified assumption of the alpha particle wave function is made. We demonstrate that previously discussed spectroscopic characteristics correspond to overlaps with cluster basis channels, using both normalized and bare channels for comparison.

While keeping in mind all of the limitations of these spectroscopic characteristics, we put forward dynamic spectroscopic factors, a natural generalization, suggesting the substitution of the static basis channels with actual dynamic RGM solutions (referred to as cluster channels).

In Sec. III present the bulk of our studies, showing how the method is used, how clustering emerges, and how it is related to cluster channels and their positions in the energy spectra. We also address the structure of various channels including those of three alpha particles. We present examples for both no-core and with-core valence spaces and corresponding Hamiltonians.

In contrast to structural overlaps between nuclear states and cluster channels that are not true observables, in Sec. IV we present an approach targeting reaction physics, where the

basis channels and extended RGM type solutions are used to obtain scattering phase shifts via the harmonic oscillator representation of scattering equations (HORSE) method. The method is extended to effectively treat the Coulomb part of the interactions and its application to ^{8}Be is shown.

A brief summary of our work is given in Sec. V.

II. CLUSTERING STRUCTURE

In this section we describe quantum many-body methods pertinent to the formulation of the resonating group method for clustering problems. The methods presented are of a structural nature and thus are limited to clustering characteristics of bound states or narrow resonances, namely those where Fermi's "golden rule" is applicable. Despite this limitation the structural form of channels described here represents a doorway for doing reaction physics with clusters; this topic is described in Sec. IV.

A. Configuration interaction

As a foundation of our many-body configuration interaction approach we use the single particle harmonic oscillator (HO) basis

$$\langle \mathbf{r}|n\ell m\rangle = \phi_{n\ell m}(r,\theta,\phi) = \frac{\phi_{n\ell}(r)}{r} Y_{\ell m}(\theta,\phi), \tag{1}$$

which are eigenstates of a spherically symmetric HO potential determined by the frequency parameter ω and mass parameter m. The characteristic oscillator length is $b = \sqrt{\hbar/m\omega}$. The corresponding energies $\hbar\omega(N+3/2)$ depend only on the frequency ω and on the total number of excitation quanta,

$$N = 2n + \ell. \tag{2}$$

The integer $n = 0, 1, \ldots$ above denotes the total number of nodes in the radial wave functions, ℓ is the orbital angular momentum, and m is its magnetic projection. The explicit forms of HO wave functions can be found in a number of textbooks [49]; details pertaining to this work and our computer codes can be found in Ref. [50].

Any multinucleon wave function that we use is represented via a linear combination of Slater determinants that in the form of second quantization is written as

$$|\Psi\rangle \equiv \Psi^\dagger|0\rangle = \sum_{\{1,2,3,\ldots A\}} \langle 1,2\ldots A|\Psi\rangle\, a_1^\dagger a_2^\dagger \ldots a_A^\dagger|0\rangle, \tag{3}$$

where $a_1^\dagger$ is a single-nucleon creation operator in a state labeled with a cumulative label 1 that combines the HO quantum numbers with a nucleon spin. In Eq. (3) we emphasize the polymorphism between states and operators by expressing the same state as a result of many-body creation operator $\Psi^\dagger$ acting on the vacuum state $|0\rangle$.

Unlike the traditional shell model which is built on a predetermined set of Slater determinants, the configuration interaction (CI) approach uses on-demand configurations. Thus, within the CI approach building the channel basis and boosting a small number of states can be done without any significant computational resources.

Relying on the commutation of operators in second quantization, the configurations in Eq. (3) are always organized under forward ordering so that $1 < 2 < \cdots < A$. The underlying operation that forward orders two configurations plays a key role in products of wave functions assuring Pauli antisymmetry between all nucleons at all stages,

$$|\mathcal{A}\{\Psi_\alpha\Psi_\beta\}\rangle = \Psi_\alpha^\dagger\Psi_\beta^\dagger|0\rangle. \tag{4}$$

Another benefit to CI comes from the ability to view configurations as a generalized object, for example the symmetry-adapted No-Core Shell Model (NCSM) [51] relies on select symmetry-based configurations. It is often the case that just a few select symmetry-based configurations play a dominant role. Combining various types of configurations, although at the expense of introducing nonorthogonality, is a major component of the CI development. In this work, as one specific type of configuration useful for establishing connection to earlier works [52], we use SU(3) symmetry-based configurations. Upon final evaluation the SU(3) configurations are converted to an m-scheme form of Eq. (3) by numerical diagonalization of the Casimir operators of SU(3) and its subgroups.

B. Center of mass

The many-body HO Hamiltonian that determines our basis states has a rich symmetry; naturally this is evident from the large degeneracy of eigenstates where energy is determined only by the total number of oscillator excitation quanta N which can be distributed among nucleons in multiple ways. All states having the same number of quanta form representations of oscillator symmetry groups. In order to respect all of these symmetries in our work, similar to no-core shell model strategies [53], any truncation of configurations is done by the number of excitation quanta. Along with the already mentioned SU(3), another symmetry group is O(A) which reflects an orthogonal transformation of all nucleon coordinates. This symmetry allows for an exact separation of the center-of-mass (c.m.) coordinate in the restricted space. Thus, while in a configuration space determined by the maximum number of oscillator excitation quanta $N_{\max}$ the total number of quanta is shared between c.m. and intrinsic degrees of freedom $N = N_{\text{c.m.}} + N'$. Using the c.m. Hamiltonian one can separate exactly the states with $N_{\text{c.m.}} = 0$, the so-called nonspurious states, so that the total wave function of type (3) has a form

$$\Psi = \phi_{000}(\mathbf{R})\Psi'. \tag{5}$$

These states, where the overall c.m. is in the lowest oscillator state, are considered to comprise a physical space of interest. Naturally, any translationally invariant operator that does not depend on the c.m. degree of freedom would be evaluated between these states as if they were evaluated using translationally invariant intrinsic wave functions Ψ'. The well-known computationally efficient procedures for separating nonspurious states were proposed by Palumbo and Prosperi and further developed by Gloeckner and Lawson [54,55].

In this work we build a basis for cluster reaction channels which are many-body wave functions of type (3) and with overall c.m. as in Eq. (5) but they are comprised of two or

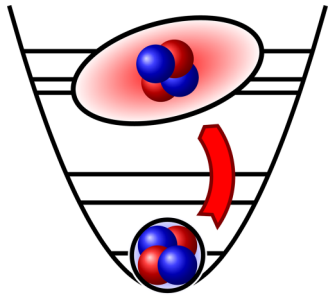

FIG. 1. Schematic depiction of the boosting process for a α particle being boosted to higher shells.

more fragments that are in a specific HO oscillator state of relative motion, with $N_{\rm rel}$ relative number of quanta. For this purpose we introduce a c.m. boosting procedure [29,56] which amounts to construction of wave functions,

$$\Psi_{n\ell m} = \phi_{n\ell m}(\mathbf{R})\,\Psi'. \tag{6}$$

The boosting procedure for the alpha particle is shown schematically in Fig. 1.

By satisfying the principles of translational invariance we maintain the exact factorization of the c.m. degree of freedom therefore operations on the c.m. coordinate discussed here have no effect on the intrinsic wave function Ψ' and its quantum numbers. Throughout this work we explicitly show the c.m. quantum numbers and quantum numbers of relative motion between c.m.'s of clusters, while the intrinsic quantum numbers are presumed to be a part of wave functions Ψ', which in every case denotes a particular nucleus or cluster.

The wave functions (6) generalize the nonspurious state in Eq. (5) since $\Psi = \Psi_{000}$. These spurious c.m.-excited states also emerge as unwanted solutions in the NCSM; though in that case effective $N'_{\rm max}$ available for the intrinsic part is reduced by the number of quanta taken by the c.m. excitation $N'_{\rm max} = N_{\rm max} - (2n + \ell)$. Difficulty in diagonalization and reduction in the $N'_{\rm max}$ make extraction of c.m.-boosted states (6) from diagonalization impractical. The strategy described next only requires a single state $\Psi = \Psi_{000}$ as input, which is obtained in a separate NCSM study.

In order to manipulate the c.m. part of the wave function we introduce c.m. creation and annihilation operators defined in the usual way:

$$\mathcal{B}^\dagger_m = \frac{1}{\sqrt{2Am\omega\hbar}}(Am\omega R_m - iP_m), \tag{7}$$

$$\mathcal{B}_m = \frac{1}{\sqrt{2Am\omega\hbar}}(Am\omega R_m + iP_m), \tag{8}$$

where m denotes a specific magnetic projection of vectors. These operators are one-body operators and are related to the isoscalar mass-density dipole ($E1$) operator,

$$D_m = \sqrt{\frac{4\pi}{3}}\sqrt{\frac{\hbar}{2AM\omega}}(\mathcal{B}^\dagger_m + \mathcal{B}_m). \tag{9}$$

The action of each creation operator increases the number of c.m. quanta by 1 and at the same time changes the rotational quantum numbers according to its vector properties. In accordance with the $N = 2n + \ell$ relation for quantum numbers of a spherically symmetric HO, the N spin-1 bosons couple to angular momenta only of the same parity $\ell = N, N-2, \ldots$ and only with multiplicity of 1, thus construction is unique and, similar to expressions of spherical Harmonics through Cartesian coordinates, can be written analytically. However, we found it more convenient to implement a simple recursive strategy as follows. Two raising operators coupled to a rotational scalar, the dot product of two vectors,

$$\boldsymbol{\mathcal{B}}^\dagger \cdot \boldsymbol{\mathcal{B}}^\dagger \equiv (\mathcal{B}^\dagger_{+1}\mathcal{B}^\dagger_{-1} + \mathcal{B}^\dagger_{-1}\mathcal{B}^\dagger_{+1} - \mathcal{B}^\dagger_0\mathcal{B}^\dagger_0), \tag{10}$$

raise the number of nodes n in the c.m. coordinate by 1 and correspondingly N by 2,

$$\boldsymbol{\mathcal{B}}^\dagger \cdot \boldsymbol{\mathcal{B}}^\dagger \Psi_{n\ell m} = \tfrac{1}{4}\sqrt{(2n+2)(2n+2\ell+3)}\;\Psi_{n+1\ell m}. \tag{11}$$

The analytically known normalization, see also Ref. [50], provides an important numerical check. In order to increment the angular momentum ℓ the easiest strategy is to move along the chain of aligned states where $m = \ell$ with sequential action of $\mathcal{B}^\dagger_{+1}$,

$$\mathcal{B}^\dagger_{+1}\Psi_{n\ell\ell} = \sqrt{\frac{(\ell+1)(2n+2\ell+3)}{4(2\ell+3)}}\Psi_{n\ell+1\ell+1}. \tag{12}$$

The angular momentum operator in this bosonic space is proportional to the cross product $\mathcal{B}^\dagger \times \mathcal{B}$, the axial vector that does not change the number of oscillator quanta. Thus, the m projection can be brought to the desired value by repeated action of an angular momentum raising and lowering operators,

$$\mathcal{L}_\pm = \pm 4\sqrt{2}(\mathcal{B}^\dagger_0\mathcal{B}_{\pm1} - \mathcal{B}^\dagger_{\pm1}\mathcal{B}_0), \tag{13}$$

following well known relations,

$$\mathcal{L}_\pm\Psi_{n\ell m} = \sqrt{(l \mp m)(l \pm m + 1)}\Psi_{n\ell m\pm1}. \tag{14}$$

A related discussion on angular momentum can be found in Refs. [35,57].

In Appendix A technical details describing the structure of c.m.-boosted states and connection with the SU(3) algebraic limit widely used in the literature are presented.

C. Basis for cluster reaction channels

Let us start our discussion here with two-body reaction channels where two clusters, with A_1 and A_2 nucleons respectively, are combined to form the $A = A_1 + A_2$ system. We use the term reaction channel following its traditional definition as an asymptotic state of the $A_1 + A_2$ system which includes states of each individual cluster with stationary wave functions $\Psi^{(1)}$ and $\Psi^{(2)}$ and the wave function of their relative motion identified by the partial wave quantum number ℓ. We assume that the wave functions for both clusters $\Psi^{(1)}$ and $\Psi^{(2)}$ are available from some previous shell model or NCSM calculations which makes their c.m.-boosted versions in Eq. (6) available as well. In our approach, which follows the standard resonating group method and, equivalent to it, the generator coordinate method [38,39], we construct the asymptotic channels as linear combinations of the *channel basis* states,

$$\Phi_{n\ell m} = \mathcal{A}\{\phi_{000}(\mathbf{R})\phi_{n\ell m}(\boldsymbol{\rho})\Psi'^{(1)}\Psi'^{(2)}\}. \tag{15}$$

Here the c.m. coordinate $\mathbf{R}$ and relative coordinate ρ are

$$\mathbf{R} = \frac{A_1\mathbf{R}_1 + A_2\mathbf{R}_2}{A_1 + A_2}, \quad \boldsymbol{\rho} = \mathbf{R}_1 - \mathbf{R}_2. \tag{16}$$

Importantly, the wave function (15) is still of the CI type that depends on coordinates of all nucleons and is expressed through linear superposition of Slater determinants following the form of second quantization in Eq. (3). Explicitly, this form is achieved via the recoupling of c.m. wave functions for two c.m.-boosted fragments into a combined state with an overall c.m. being in the nonspurious state while relative motion is in HO state with quantum numbers $n\ell m$. The recoupled channel basis wave function in Eq. (15) is created using the second quantization rules discussed earlier, see Eq. (4), by the following operator:

$$\Phi^\dagger_{n\ell} = \sum_{\substack{n_1\ell_1\\ n_2\ell_2}} \mathcal{M}^{n\ell 00;\ell}_{n_1\ell_1 n_2\ell_2} \left[\Psi^\dagger_{n_1\ell_1 m_1} \times \Psi^\dagger_{n_2\ell_2 m_2}\right]_\ell \tag{17}$$

with $\mathcal{M}^{n\ell 00;\ell}_{n_1\ell_1 n_2\ell_2}$ being the oscillator bracket also known as the Talmi-Moshinsky-Smirnov coefficient [58]. In Eq. (17) we slightly generalize Eq. (15) and introduce an abbreviated notation ℓ that denotes all asymptotic channel quantum numbers. The RGM basis channels do not need to have any specific symmetry or spin coupling. The situation is similar to the basis states within a traditional shell model. The fundamental symmetries are automatically maintained and restored by the Hamiltonian, as long as all relevant basis channel states are included. The best choice may be dictated by anything from theoretical considerations to actual experimental setup. Thus, in each particular example the set of asymptotic quantum numbers is different and identified separately. The bulk of this work deals with spinless α particles, $J_1 = 0$; in this case the asymptotic state can be identified by the partial wave ℓ, its magnetic projection m, and angular momentum state of the second fragment J_2 and M_2. We also used an equivalent set of basis channels where J_2 and angular momentum ℓ are coupled to a total channel angular momentum J. Thus, the square brackets in Eq. (17) denote all the desired spin and angular momenta couplings.

Discussing multifragment clustering, both ℓ and internal index n have to be further generalized. In particular, while for the two-body problem $A_1 + A_2$ in Eq. (17) we used n to denote the number of nodes in the relative HO wave function, which is equivalent to using the total number of oscillator quanta in relative motion $N_{\rm rel} = 2n + \ell$. In general, we view n as an index that labels channel basis states, for example for three cluster channels a single total number of quanta in relative motion $N_{\rm rel}$ is insufficient to label a three-body state. The three-α channel basis states discussed below are constructed via sequential coupling, building relative Jacobi coordinates. An alternative method is to just numerically solve a three-boson problem in the HO basis with the Hamiltonian containing Casimir operators of symmetries involved, and thus obtaining all nonspurious solutions of angular momenta of interest. This would automatically provide a numerical form of generalized coefficients $\mathcal{M}$ coupling oscillator symmetry and rotational symmetry simultaneously,

$$\Phi^\dagger_{n\ell} = \sum_{\substack{n_1\ell_1 m_1\\ n_2\ell_2 m_2\\ n_3\ell_3 m_3}} \mathcal{M}^{n\ell}_{n_1\ell_1 m_1 n_2\ell_2 m_2 n_3\ell_3 m_3} \Psi^\dagger_{n_1\ell_1 m_1} \Psi^\dagger_{n_2\ell_2 m_2} \Psi^\dagger_{n_3\ell_2 m_3}. \tag{18}$$

The diagonalization method is commonly used as a faster and more numerically stable alternative for obtaining recoupling coefficients, including oscillator brackets and Clebsch-Gordan coefficients [52,59,60].

Basis channels provide some simple, although crude, means for evaluating clustering spectroscopic characteristics; some of these characteristics, such as traditional spectroscopic factors or those from orthogonality conditions model (OCM), are used to compare our method with what has been traditionally used. We review these techniques and their connection with our work in Appendix B.

The set of basis channels is not an orthonormal basis set. The lack of orthogonality is naturally caused by the internal structure of clusters where individual nucleons are subject to Pauli blocking and antisymmetrization; this topic is reviewed in Appendix C.

D. Resonating group method

The resonating group method that we discuss next has a long history of success [61]. In recent years, the RGM has reemerged [62] as one of the leading methods to tackle the structure-reaction interface in microscopic many-body calculations. It amounts to the construction of a channel wave function,

$$|\Psi^{(\ell,\mathrm{RGM})}\rangle = \sum_n \chi_n |\Phi_{n\ell}\rangle, \tag{19}$$

variationally, where the RGM equation for the amplitudes χ_n can be written in matrix form for each asymptotic channel ℓ as

$$\sum_{n'} \mathcal{H}_{nn'}\chi_{n'} = E \sum_{n'} \mathcal{N}_{nn'}\chi_{n'}. \tag{20}$$

In this expression $\mathcal{H}$ and $\mathcal{N}$ are referred to as the Hamiltonian and norm kernel respectively and χ is a vector of variational amplitudes. The kernels are evaluated in the channel basis

$$\mathcal{H}_{nn'} = \langle\Phi_{n\ell}|H|\Phi_{n'\ell}\rangle, \quad \mathcal{N}_{nn'} = \langle\Phi_{n\ell}|\Phi_{n'\ell}\rangle. \tag{21}$$

The RGM wave functions obtained in this way are fully antisymmetrized, nonspurious, and respect all the symmetries of the Hamiltonian provided. This procedure described above is not in any way restricted to binary systems; multichannel reactions and intrinsic excitations can be included as well. For further discussion and more examples the reader is referred to Ref. [61].

The RGM channels allow us to further improve the definition of the spectroscopic factors defining them as

$$S^{(\mathrm{RGM})}_{\beta,\ell} \equiv \left|\left\langle\Psi^{(A)}\middle|\Psi^{(\ell,\mathrm{RGM})}_\beta\right\rangle\right|^2. \tag{22}$$

Here β denotes a particular RGM solution of the generalized eigenvalue problem (20). The net level of clustering is still characterized by Eq. (C4) since the RGM-defined dynamic

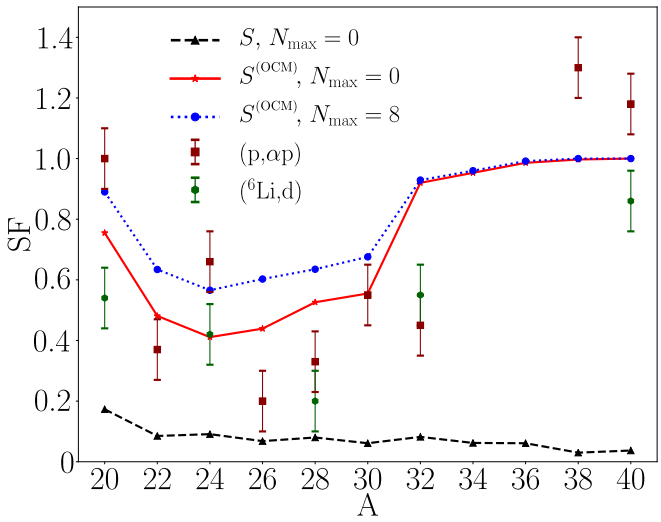

FIG. 2. Spectroscopic factors for ground state to ground state α transition $A \to (A-4)+\alpha$ for nuclei in *sd* valence with equal number of protons and neutrons. Scattered points show experimental data from knockout and pickup reactions, Refs. [37,68]. Connected points show theoretical results obtained using USDB [67] Hamiltonian; the wave function of α particle is obtained using the NCSM with JISP16 interaction, $\hbar\omega = 14$ MeV, and $N_{\max}$ as labeled. Traditional spectroscopic factors (SFs), Eq. (B3), are shown with dashed (black) line, the OCM [equivalent to RGM, Eq. (23)] SFs Eq. (C4) are in solid (red), and dotted (blue) for different truncations $N_{\max}$ of the α wave function.

channels are formed by an orthogonal transformation of orthonormalized states

$$S_\ell^{(\mathrm{RGM})} \equiv \sum_\beta \left|\left\langle \Psi^{(A)} \middle| \Psi_\beta^{(\ell,\mathrm{RGM})} \right\rangle\right|^2 = S_\ell^{(\mathrm{OCM})}. \tag{23}$$

III. EXAMPLES

A. Spectroscopic factors in *sd* space

Numerous studies of clustering have been done using the traditional shell model [34,63]. Despite being phenomenological in nature, the traditional shell model has been very successful in identifying and predicting a plethora of properties and to this day it remains a powerful tool for bridging fundamental theory and observations. Recent systematic studies and comparisons with experiment have clearly affirmed the applicability of the approach presented in preceding sections and moved the discussion to a much more quantitative level. Studies of ^{16}O in Ref. [52], ^{10}Be [64,65], ^{18}O [15], and a recent comprehensive examination of ^{20}Ne [66] validate the approach and raise some common questions which we discuss next. The studies shown in Fig. 2 use a well established semiempirical shell model Hamiltonian from Ref. [67] and show the traditional, Eq. (B3), and OCM, Eq. (C4), spectroscopic factors for ground state to ground state transitions. Below we summarize some key results of this study.

First, the traditional spectroscopic factors, while providing some relative clustering information for states within a single nucleus, generally fail to capture the systematics. This is seen in Fig. 2 where traditional spectroscopic factors, shown with a dashed (black) line, are too small and do not follow the experimentally observed trend as the mass number increases. The same findings were reported in several recent publications; for example see Ref. [52]. The OCM spectroscopic factors, on the other hand, are consistent with experimental trends.

Second, due to the phenomenological nature of the model, previous considerations employed an s^4 structure of the α particle which, as discussed in Appendix A, allows for the algebraic approach based on SU(3) symmetry. The shell model is defined via matrix elements in the configuration space, and the best agreement with data for various observables is generally achieved with oscillator frequency $\hbar\omega = 41A^{-1/3}$ MeV. For most nuclei this is not consistent with the optimal oscillator frequency for the α particle, $\hbar\omega = 20$–30 MeV; see Fig. 12. Thus, considering components of the transfer operator beyond s^4 is important. In Fig. 2 curves drawn with solid (red) and dotted (blue) lines show the OCM SF for an α particle wave function obtained within $N_{\max} = 0$ and 8 truncations, respectively. The increase in wave function complexity arising from the extra components leads to an overall increase of the SF but it is difficult to draw any specific conclusion.

Third, within a single oscillator shell only one basis channel contributes which makes OCM and RGM spectroscopic factors identical and equivalent to the traditional spectroscopic factor being normalized to unity [52]. Furthermore, beyond the single shell for $N_{\max} \neq 0$, a phenomenological shell model Hamiltonian typically does not lead to strong mixing between different particle-hole excitations. Therefore, the OCM and RGM channel wave functions are close, with oscillator wave function approximating the relative motion.

Following these comments, and in order to facilitate phenomenological studies in the *sd* shell, we can envision an effective four-body operator that in the restricted space would describe the removal or addition of an α particle. We limit this discussion to $\ell = 0$ which, due to the absence of the centrifugal barrier, would be the most important channel. An effective operator for $\ell = 0$ with $L = S = T = 0$ and appropriate permutational symmetry can be constructed in four different ways in *sd* space. It is convenient to expand the effective operator using SU(3) symmetry then the four operators possible have $(\lambda, \mu) = (8,0)$, (4,2), (0,4), or (2,0). In the algebraic limit expressed by Eq. (A1) only the (8,0) component is present and only the basis channel with $n = 4$ nodes contributes; the total norm squared of this component is given by the cluster coefficient $\left(X_{N=8}^{\eta=(sd)^4}\right)^2 = 1/26 \approx 0.038$ as listed in Table VII. The results in Table I show changes when we depart from the algebraic limit and consider a realistic α computed for the oscillator frequency of $\hbar\omega = 14$ MeV that is better suited for *sd*-shell nuclei. Basis channels with different numbers of nodes contribute and components other than $(\lambda\mu) = (8,0)$ appear. Table I therefore represents a form of an effective α transfer operator for the *sd* space. Departure from the algebraic limit and the presence of small components are important in studies of numerous unexplained hindered α transitions such as those discussed in [69] This result is also a good starting point for phenomenological determination of parameters in Table I.

TABLE I. SU(3) decomposition of basis α cluster channels for different numbers of nodes. The second column lists the total normalization squared of the operator in the *sd* space, X^2; the remaining columns labeled with $(\lambda\mu)$ show weights of the corresponding SU(3) components. The α particle structure is computed using oscillator frequency $\hbar\omega = 14$ MeV in an $N_{\max} = 8$ space using JISP16 interaction. Channels are identified by the number of nodes in the relative wave function shown in the first column, only $\ell = 0$ partial wave is discussed.

n	X^2	(8,0)	(4,2)	(0,4)	(2,0)
4	0.02848	1.0	0.0	0.0	0.0
3	0.006 97	0.561 658	0.438 338	0.0	0.0
2	0.001 69	0.549 804	0.045 184 7	0.3363	0.0 636 439
1	0.000 18	0.0 693 304	0.735 878	0.0134 005	0.1 47 418
0	0.000 11	0.0 693 304	0.261 291	0.0 990 471	0.0 384 533

B. Case of ^{20}Ne

Continuing our discussion in the previous subsection, we consider the distribution of α spectroscopic strength within a specific nucleus. Distribution of the clustering strength and going beyond statistical approaches is important in astrophysical studies [70,71]. Here we concentrate on ^{20}Ne, a classic benchmark in studies of clustering, and a good example of both successes and limitations of the traditional shell model [66,72–74]. Under the assumption of s^4 structure of the α, the ground state SF is large (0.76) and consistent with observations for this and neighboring nuclei (^{22}Ne, ^{24}Mg), indicating that the high degree of clusterization observed is reproduced by the shell model calculation. All the members of the ground state rotational band can be described as an α particle orbiting the closed ^{16}O core in a specific ℓ state. The α SF to the ground state of ^{16}O, along with the reduced transition rates for the deexcitation of each state $[B(E2)\downarrow]$, are shown in Table II. The yrast states show both a rotational behavior and α cluster characteristics. For each state there is only one channel, therefore RGM and OCM SF are equivalent.

The observed band is a textbook example of quadrupole collectivity [75]; microscopically the states are members of (8,0) SU(3) irreducible representation.

The formalism holds up well for negative parity states generated from one particle-hole (ph) excitations in a *p-sd-pf* space. Studies using the PSDPF [76] interaction agree at a qualitative level with the results seen in a (^{6}Li, d) reaction [77,78]. Out of over 60 states in the energy region of up to 12 MeV in excitation only the strongly clustered, natural parity, ones are populated. Detailed discussion and cross sections can be found in Ref. [50].

TABLE II. Transition rates (in Weisskopf units) and α spectroscopic factors for the ^{20}Ne rotational band members with the USDB interaction with effective charges 1.35 and 0.35, for protons and neutrons, respectively. The s^4 structure of the α is assumed.

J^π	$B(E2)\downarrow$ (W.u.) USDB	$B(E2)\downarrow$ (W.u.) Expt.	α SF(^{16}O g.s.)
0^+			0.76
2^+	14.4	20.3	0.78
4^+	17.0	22	0.66
6^+	12.7	20	0.58
8^+	8.6	9.0	0.40

TABLE III. Summary of proton and alpha spectroscopic information for the lowest $T = 0$ states. Experimental data [66] are compared with results from a shell model calculation with the USDB Hamiltonian [67]. Each state is further decomposed in SU(3) irreps. The s^4 structure of the α is assumed.

	E_x	SF (p)	(8,0)	(4,2)	(0,4)	(2,0)
0^+_1	0	0.484	0.755	0.058	0.047	0.000
0^+_2	6.698	0.574	0.142	0.550	0.162	0.000
0^+_3	11.908	0.013	0.002	0.214	0.549	0.003
0^+_5	14.665	0.010	0.025	0.103	0.000	0.020
0^+_6	16.268	0.002	0.000	0.005	0.026	0.577

When it comes to other high-lying states the situation is much more involved. Let us consider the series of the lowest 0^+ states. Table III shows the summary of SF for both alpha and the proton; see also [66] for lowest 0^+ states in different models and comparison with experimental data. Here we continue to assume the s^4 structure for the α particle making the SU(3) symmetry a defining characteristic.

The table shows that while for the lowest states dominated by configurations from a single shell the agreement is nearly excellent, some higher-lying broad alpha clustering state is difficult to describe. The same discrepancy for high-lying strongly clustered resonant states has been seen in other nuclei such as ^{18}O [15].

In Fig. 3 we move away from the algebraic limit and take more channels into account. We relax the s^4 assumption for the α particle wave function and show the distribution of RGM α SF from Eq. (23). We consider the $\ell = 0$ partial wave

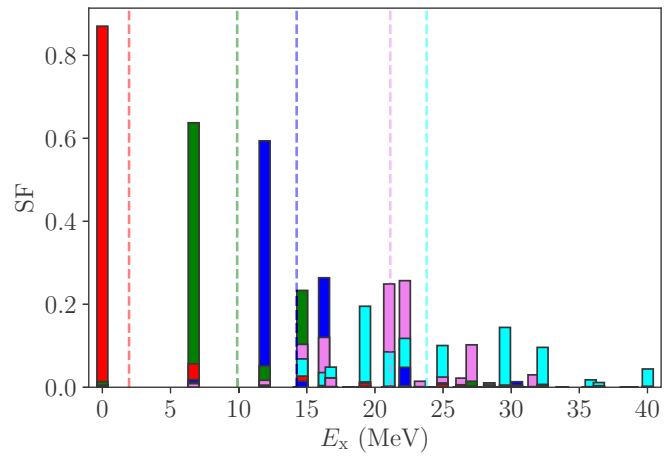

FIG. 3. Distribution of dynamic spectroscopic factors for $^{20}\text{Ne} \rightarrow {}^{16}\text{O}$ (g.s.) $+ \alpha$ with the USDB interaction. The dashed lines correspond to the RGM energies for each decay channel. The spectroscopic factors are shown using stacked components reflecting each individual RGM channel in sum (23).

and five basis channels with $n = 0, 1, 2, 3, 4$. These are the only contributing channels with components in the *sd* space with $N = 8$ oscillator quanta. This leads to five RGM energies which are shown with dashed vertical lines and the sum over partial SF in Eq. (23) is shown by a stacked histogram using corresponding color and style.

In agreement with the previous discussion the ground state SF is dominated by a single channel which is structurally close to the $n = 2$ basis channel (shown in red). Similarly the SFs for the following two excited states are dominated by single channels, however fragmentation is rapidly increasing with excitation. It is remarkable that the clustering strength is concentrated near the RGM energies. If one loosely associates RGM solutions as representing thresholds for each new bound α state in a crude potential model then this result can be seen as supporting the near-threshold increase in clustering strength discussed extensively in the literature [6,79,80].

C. ^{21}Ne, weak coupling limit $^{16}\mathrm{O} + \alpha + n$

Molecular-type dynamics where much-heavier clusters along with light single nucleons form structures similar to those of molecules have been discussed for some time [6,9]. Whether such structures can emerge in CI approaches is of interest. Let us view the nucleus ^{20}Ne as a core + α system which from the preceding discussion is known to be clustered. To investigate how the system responds to an extra nucleon, we take channels created to have a $^{16}\mathrm{O} + \alpha$ structure with relative angular momentum $\ell = 0, 2, 4, 6$ and add a neutron in the $d_{5/2}$ orbital, recoupling to all possible angular momenta in each case. Alternatively, one can consider adding an α particle with a definite relative motion to the ground state of ^{17}O. We end up with 18 channel basis states (configurations) versus the 1935 $m = 1/2$ many-body shell model basis states. This idea of reducing the size of the problem using cluster configurations instead of all the many-body states possible in the space is at the center of interest in the configuration interaction strategies and in the cluster-nucleon configuration interaction approach, Ref. [52].

In the smaller subspace of these (nonorthogonal) basis channels, we apply the resonating group method approach and solve the generalized eigenvalue problem, with the matrix elements of the Hamiltonian Kernel calculated with the USDB interaction. This is equivalent to CI limited to the cluster basis. The resulting low-lying spectrum is compared with both the USDB shell model and experimental values in Fig. 4.

The RGM reproduces the excitation spectrum quite well, but the binding is 3.5 MeV lower than the full USDB calculation, the latter being close to experiment. The discrepancy is to be expected from the variational approach. Considering that only 18 basis wave functions are being used with only a few for each spin, the quality of agreement is remarkable. Furthermore, from the configuration mixing in cluster channels we infer that the simple picture of an α particle moving in some definite partial wave relative to ^{16}O and the extra nucleon being a spectator is perturbed. For example the ground state $3/2^+$ is a mixture of $\ell = 2$ and $\ell = 4$ components. Similarly, the excited $5/2^+$ is a nearly equal mixture of $\ell = 0$ and $\ell = 4$. This mixing has been probed using experiments with transfer

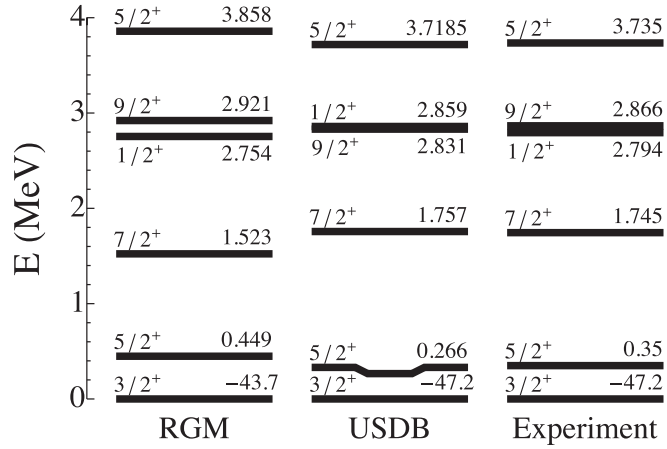

FIG. 4. Low-lying RGM, full USDB SM, and experimental spectra of ^{21}Ne. The ground states show total binding energy; the excitation energies are shown for all of the remaining excited states, all in units of MeV.

reactions, Ref. [81]. The comparison of α SF is shown in Table IV, where, following the way the experimental data were presented in Ref. [81], the SF are normalized to the $\ell = 2$ partial wave of the ground state transfer. The experimental $J^\pi = 9/2^+$ values are grouped together with the ones for the $1/2^+$ state because they are difficult to resolve due to their small energy difference.

In order to quantify the mixing we provide here the components of the generalized eigenvalue problem in the sector with spin-parity quantum number $5/2^+$. The basis states can be labeled with $\ell = 0, 2, 4$ (we present them in this order) so that each $J^\pi = 5/2^+$ basis state is obtained from coupling with a neutron on $d_{5/2}$ orbit as $(\ell \times 5/2)_{5/2}$. The norm kernel

$$\mathcal{N} = \begin{pmatrix} 0.185 & -0.03 & -0.038 \\ -0.03 & 0.170 & -0.015 \\ -0.038 & -0.015 & 0.219 \end{pmatrix} \tag{24}$$

demonstrates that the basis channels are not orthogonal although off-diagonal matrix elements are an order of magnitude smaller than those on the diagonal. For the Hamiltonian kernel, transformed using the norm kernel to represent a

TABLE IV. Comparison between the experimental SF (upper table) and RGM SF (lower table) for low-lying states in ^{21}Ne.

$\mathcal{S}^{(\mathrm{expt.})}$	$3/2^+$	$5/2^+$	$7/2^+$	$9/2^+, 1/2^+$
$\ell = 0$		1.04 ± 0.41		
$\ell = 2$	1.0 ± 0.05	...	0.91 ± 0.08	0.9 ± 0.05
$\ell = 4$	0.42 ± 0.04	0.32 ± 0.18	0.23 ± 0.04	0.29 ± 0.03
$\mathcal{S}^{(\mathrm{RGM})}$				
$\ell = 0$		0.78		
$\ell = 2$	1.0	0.02	0.9	0.81
$\ell = 4$	0.18	0.44	0.14	0.33

TABLE V. Experimental data and theoretical results for ^{8}Be. All energies and widths are given in units of MeV except for the widths marked with $*$; those are presented in units of eV.

ℓ	$E_{\rm ex}$	Γ	$E_{\rm ex}^{\rm (RGM)}$	$\Gamma^{\rm (RGM)}$	$\mathcal{S}^{\rm (RGM)}$
0	0.0	5.6*	0	8.9*	0.69
2	3.0	1.5	4.6	1.4	0.66
4	11.4	3.5	16.0	2.7	0.51

Hermitian eigenvalue problem,

$$\tilde{\mathcal{H}} = \mathcal{N}^{-1/2}\mathcal{H}\mathcal{N}^{-1/2} = \begin{pmatrix} -42.1 & 0.20 & 1.79 \\ 0.20 & -39.9 & -0.15 \\ 1.79 & -0.15 & -40.3 \end{pmatrix}, \quad (25)$$

we find strong mixing. Here all matrix elements are given in units of MeV and rows (columns) correspond to intermediate coupling momentum ℓ in order $\ell = 0, 2, 4$. The mixing between $\ell = 0$ and $\ell = 4$ lowers the energy of the first excited state by approximately 1.2 MeV.

D. ^{8}Be in no-core CI approach

The ^{8}Be nucleus and its structure as $^8\text{Be} \rightarrow \alpha + \alpha$ is a classic benchmarking case in studies of nuclear clustering [41,44,79,82–84]. In Table V we list experimental energies and widths, and our results, discussed later, for the sequence of 0^+, 2^+, and 4^+ clustered resonances in ^{8}Be. These states form a clustering rotational band where two alphas are in the state of motion with the relative angular momentum $\ell = 0$, $\ell = 2$, and $\ell = 4$, respectively. The sequence with the ground state being nearly bound (with a decay width of 5.6 eV) and the 4^+ excited state being a broad resonance is a perfect arena for the structure-reaction transitional physics to be explored.

Following our strategy described in Sec. II D for each partial wave ℓ we construct a set of basis channels labeled by n which is the number of nodes in the relative $\alpha + \alpha$ wave function. Under an assumption of trivial s^4 configuration for each of the α particles (equivalently, $N_{\rm max} = 0$ in the NCSM) the norm kernel is diagonal; see Eq. (C2). For example, in the spin-parity subspace 0^+ and considering only three channels with $n = 2, 3$, and 4 the normalized Hamiltonian kernel for the JISP16 interaction with $\hbar\omega = 25$ MeV is

$$\tilde{\mathcal{H}} = \begin{pmatrix} -15.12 & 19.68 & -0.629 \\ 19.68 & 16.74 & 32.77 \\ -0.629 & 32.77 & 47.72 \end{pmatrix}. \quad (26)$$

Here the minimal number of nodes is determined by the minimal total number of quanta $N = 2n + \ell = 4$, which enforces Pauli blocking. With increasing number of quanta in relative motion the normalized kinetic energy should reach the asymptotic value corresponding to the relative kinetic energy

$$\tilde{T}_{\rm NN} = (N + 3/2)\frac{\hbar\omega}{2} + 2T(\alpha), \quad (27)$$

where $T(\alpha)$ is the intrinsic relative kinetic energy of each α particle; $T(\alpha) = 9\hbar\omega/4$ for the s^4 configuration. The kinetic energy operator in the HO basis is tridiagonal, which explains

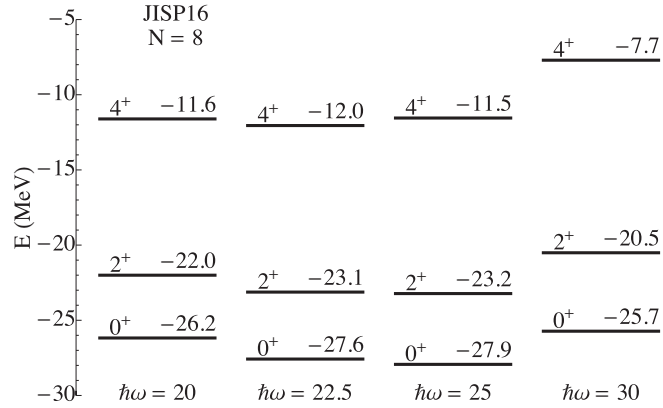

FIG. 5. RGM spectra showing rotational band of ^{8}Be for various values of $\hbar\omega$ with the JISP16 interaction. All energies are shown in units of MeV.

the magnitude of the matrix elements in Eq. (26), the asymptotic form of Hamiltonian and norm kernel is further discussed in Sec. IV. The RGM excitation spectrum that follows from the JISP16 interaction with optimal $\hbar\omega = 25$ MeV is included in Table V. We use the JISP16 interaction, allowing for up to 12 quanta in each ℓ channel.

Let us emphasize the emergence of the cluster rotational band in the RGM solution. In Table V the ratio of excitation energies of 4^+ to 2^+ is $R_{42} \approx 3.5$ which is close to the 3.3 value expected for a rotational band where $E_{\rm ex} \propto \ell(\ell + 1)$. The $\hbar\omega$ dependence of the approach is studied in Refs. [21,50,85]; here we summarize the results using Fig. 5. The presence of the rotational band is robust and the s^4 approximation for alpha particles favors a specific frequency $\hbar\omega \approx 25$ MeV where energies are minimized due to the variational nature of the approach.

As mentioned earlier, the $N_{\rm max} = 0$ treatment of the alpha particles, and in general so called "s clusters" that carry no oscillator quanta ($N = 0$), allow for a relatively simple algebraic treatment which is widely used by many authors in Refs. [34,35,52,86,87]. In this limit our results have been verified to be identical. However, the d-wave component of the alpha particle and the preference for a different oscillator parameters for describing relative motion or structure of parent and/or daughter systems in cases of alpha decay, see Sec. III A, point to a potential benefit in going away from this simple limit. The advantage of our approach is that apart from increasing computational difficulty it remains unchanged for any type of clustering. In order to find an optimal strategy we study the RGM spectrum as a function of $N_{\rm max}(\alpha)$ and $N_{\rm max}({\rm rel})$ which are the maximum number of quanta in the wave function of each alpha particle and the maximum number of quanta in relative motion, respectively. We will not address here computational strategies, but we assume that the total computational difficulty roughly scales as $N_{\rm max} = 2N_{\rm max}(\alpha) + N_{\rm max}({\rm rel})$ for the $\alpha + \alpha$ case. In Fig. 6, we show the RGM spectra for a fixed $\hbar\omega = 20$ grouped by $N_{\rm max}(\alpha)$ and $N_{\rm max}({\rm rel})$, as labeled. All of the spectra show a well-formed rotational band, however the ground state energy is different and considering $N_{\rm max}(\alpha)$ and $N_{\rm max}({\rm rel})$ as

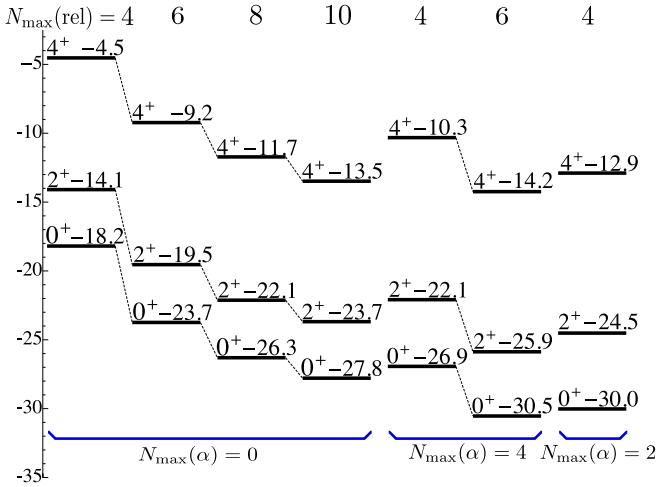

FIG. 6. RGM calculations of the rotational band of ^{8}Be for $\hbar\omega =$ 20 MeV with the JISP16 interaction and with the α particle wave function taken from a NCSM calculation with the corresponding value of $N_{\max}$. The value N in the plot reflects the total number of HO quanta available to the relative motion between the two clusters.

parameters of the variational treatment we find that the combination $\hbar\omega = 20$ MeV and $N_{\max}(\alpha) = 2$ seems to be optimal. While the question about optimal $N_{\max}$ truncation and optimal HO frequency has to be investigated further, our studies suggest using $N_{\max}(\alpha) = 2$.

In Fig. 7 we show the form of the radial s-wave wave function for the relative $\alpha + \alpha$ motion defined using the radial parts of HO wave functions $\phi_{n\ell}(\rho)$ in Eq. (1) and the RGM solution in Eq. (20),

$$u_\ell(\rho) = \sum_n \chi_n \phi_{n\ell}(\rho). \tag{28}$$

The $\ell = 0$ channel is shown where we select different values of $\hbar\omega$ to highlight the sensitivity of the results to the HO parameter.

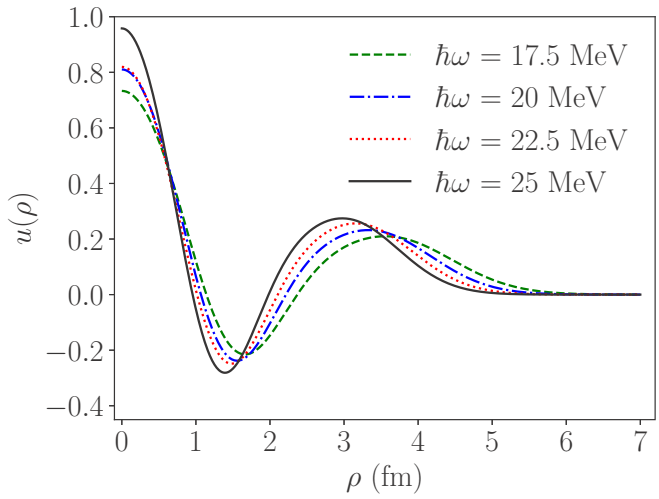

FIG. 7. Relative $\alpha + \alpha$ wave function for the 0^+ RGM channel in ^{8}Be calculated with the JISP16 interaction. Different curves correspond to different oscillator parameter $\hbar\omega$ as labeled.

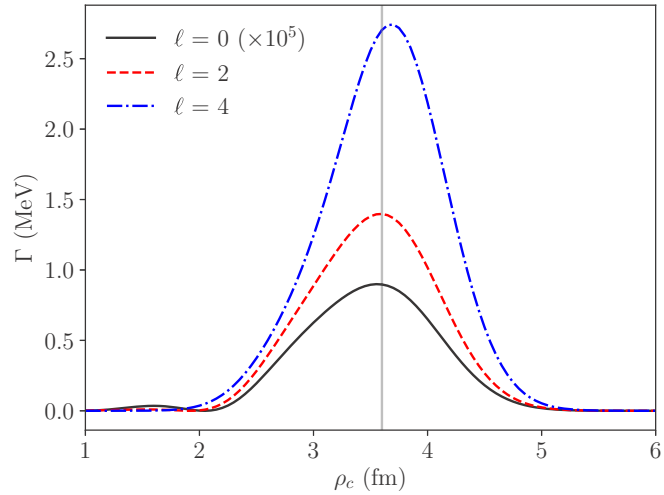

FIG. 8. Dependence of the width of each resonance in ^{8}Be with varying channel radius. The vertical line corresponds to the chosen $\rho_c = 3.6$ fm value. The width for the 0^+ resonance is magnified by a factor of 10^5 in order to be visible.

Our structural treatment should be appropriate for the extremely narrow ground state; at the same time one should keep in mind that projection of a many-body problem onto the dynamics of two alphas is observed experimentally only via scattering observables. Additionally one should be wary of a common issue related to binding energies and thresholds; certainly microscopic approaches utilizing fundamental nucleon-nucleon interactions provide remarkable precision but it is unrealistic to expect these models to work at the level of kilovolt precision necessary to describe the 91.8-keV alpha decay Q value of ^{8}Be. This is not a problem, however, because the structure of the wave function does not change significantly within a reasonable energy interval near threshold [88]. Formally, in this limit structure and reaction questions are separated, and coupling to the continuum can be treated within the lowest order of perturbation theory [89]. We used this approach for determining the decay widths in Table V; here the standard R-matrix equation was used [90,91],

$$\Gamma_\ell = \frac{\hbar^2 k}{\mu} \frac{\rho_c^2 u_\ell^2(\rho_c)}{F_\ell^2(\eta, k\rho_c) + G_\ell^2(\eta, k\rho_c)}, \tag{29}$$

where the channel radius was selected at $\rho_c = 3.6$ fm. With this choice, the width as a function of radius reaches its maximum, maximizing the outgoing flux into the decay channel, and in the vicinity of the extremum there is minimal sensitivity to the channel radius; see Fig. 8. It is remarkable that nearly the same channel radius is appropriate for all members of the rotational 0^+, 2^+, and 4^+ members of the band, suggesting a rigid nature of the rotating system. For narrow resonances this is known to be a good approximate method [89,92] and it works well for ^{8}Be; see Table V.

Studies of ^{8}Be have been conducted using other no-core interactions including obtained with similarity renormalization group (SRG); see [50]. While there are some differences, especially in binding energies, the channel structure, spectroscopic factors, and even effective moment of inertia for the

TABLE VI. Excitation energies (in MeV) for rotational band members in ^{12}C, experiment, NCSM, and RGM both with $\hbar\omega =$ 25 MeV, followed by spectroscopic factor for triple alpha decay. The last column shows the number of basis channels included in the calculation.

J^π	$E_{\rm ex}^{\rm (expt.)}$	$E_{\rm ex}^{\rm (NCSM)}$	$E_{\rm ex}^{\rm (RGM)}$	$\mathcal{S}_\ell^{\rm (RGM)}$	Channels
0^+	0	0	0	0.42	8
2^+	4.4	6.06	3.61	0.49	16
4^+	14.1	19.8	13.6	0.6	16

$0^+, 2^+, 4^+$ band remain nearly unchanged. All of this supports the experimentally observed picture of these states being resonant scattering states of two alphas.

E. Triple α clustering in ^{12}C

Alpha clustering plays an important role in structure and reactions involving ^{12}C. Different geometrical configurations of alphas have been discussed in Refs. [43,93,94] and signatures of the alpha condensate have been searched for [46,48]. In addition, the coupling of the first excited 0^+ state, named after F. Hoyle, to a triple-alpha open decay channel is of paramount importance for formation of elements in the universe. We concentrate on the structure of the triple-alpha decay channel and comment on the clustering structure of the lowest excited 0^+ state. The Hoyle state is unbound by 285 keV and thus the process $^{12}\mathrm{C} \to \alpha + \alpha + \alpha$ can proceed via an intermediate ^{8}Be resonance, which as discussed earlier is only 93 keV above the threshold. The decay via an intermediate ^{8}Be is, in fact, what happens nearly 100% of time [25–28]. Certainly such an overwhelming probability comes mainly from three-body Coulomb final state dynamics which favors tunneling of a single alpha first. Here we discuss structural questions that determine transition amplitudes between initial states and final channels.

The basis channels involving three clusters of the form (18) are built using a sequential pair-wise coupling procedure for two internal Jacobi coordinates. We allow up to $N_{\rm max}({\rm rel}) =$ 12 oscillator quanta of relative motion to be shared amongst the two relative coordinates. We employ the RGM procedure with three identical α particles, each in an s^4 configuration using the JISP16 interaction with $\hbar\omega = 25$ MeV. The minimum allowed by the exclusion principle is $N_{\rm rel} = 8$; this basis channel with $J^\pi = 0^+$ represents a configuration with a filled $0s$ shell and eight nucleons in the $0p$ shell; normalization can be found in Table IX. For each of the following $N_{\rm rel}$ the number of basis channels is shown in Table VI.

Table VI shows that the NCSM predicts the lowest 0^+, 2^+, and 4^+ to be strongly clustered. While it is hard to rely on the NCSM for the structure of the Hoyle state here the SF $\mathcal{S}^{\rm (RGM)}(0_2^+) = 0.257$ which, coincidentally, is a reasonable value. The overlaps squared between the triple-alpha channel with quantum numbers 0^+ and a two-fragment channel constructed from the ground state of ^{8}Be ($N_{\rm max} = 4$) and an α in relative motion with $n = 2$ and $\ell = 0$ is 0.51. This high overlap emphasizes that the decay process going through an intermediate ^{8}Be state is most probable; apart from the overlap the binary channel is strongly favored by the kinematics of the three-body Coulomb problem.

IV. REACTIONS WITH CLUSTERS

In the preceding presentation we established clustering channels and demonstrated how these channels can be used to obtain spectroscopic factors and other structural characteristics of clustering that are relevant for bound states and in the limit of weak continuum coupling [95]. The channels also provide a formal path for dealing with cluster reactions, which is our next subject. Here we discuss two-body reaction processes. Formally, the same techniques can be applied to more complicated reactions however, the difficulty, both theoretical and experimental, in building and studying multifragment asymptotic states puts the more complicated reactions outside the scope of this presentation. On the other hand, two-body scattering, especially the case involving a spinless particle, is a standard textbook example of partial wave analysis [88]. The starting point for the following will be the radial problem in the space of radial wave functions describing the separation of two clusters for a given fixed partial wave ℓ. The asymptotic ($r \to \infty$) form of the effective Hamiltonian operator in this case includes a centrifugal term in addition to the usual long-range Coulomb,

$$H^0 = -\frac{\hbar^2}{2\mu}\frac{d^2}{dr^2} + \frac{Z_1 Z_2 e^2}{r} + \frac{\hbar^2 \ell(\ell+1)}{2\mu r^2}. \tag{30}$$

The asymptotic solution at a given energy E can be written as a linear superposition of a regular $F_\ell(\eta, kr)$ and an irregular function $G_\ell(\eta, kr)$,

$$\psi_\ell(r) \simeq \alpha F_\ell(\eta, kr) + \beta G_\ell(\eta, kr). \tag{31}$$

Here, $k = \sqrt{2\mu E}/\hbar$, $\eta = Z_1 Z_2 e^2 \mu/\hbar^2 k$, and $\tan\delta_\ell = \beta/\alpha$ is the phase shift. The functions F_ℓ and G_ℓ are known as the regular and irregular Coulomb functions, respectively; they are known analytically and discussed extensively in the literature [96]. For the scattering of neutral particles $\eta = 0$, and the Coulomb functions become $F_\ell(0, x) = x j_\ell(x)$ and $G_\ell(0, x) = -x n_\ell(x)$, with j_ℓ and n_ℓ being the spherical Bessel and Neumann functions.

In the context of our previous discussion it is natural to proceed in HO basis and continue to rely on the expansion of the radial motion in HO functions in Eq. (28).

Unlike the case of deeply bound states, for weakly bound and scattering states the HO expansion appears to be a poor choice, but knowledge of the analytic form of basis functions remediates this issue. The J-matrix method, Ref. [97], also known as harmonic oscillator representation of scattering equations (HORSE) [40,98] has been broadly discussed in the literature [97]. In its traditional form the method is limited to H^0 being the kinetic energy operator; our approach, discussed in what follows, is different in allowing for a Coulomb interaction to be a part of H^0, as defined in Eq. (30). The Coulomb problem represents a significant difficulty for the standard J-matrix/HORSE methods; another strategy for dealing with Coulomb interaction is discussed in Refs. [40,98].

The integer n in Eq. (28), used to enumerate the basis states, coincides with the number of nodes in the radial part

of the wave function. The method relies on the asymptotic limit of $r \to \infty$ in coordinate space being equivalent to the configuration space limit of $n \to \infty$. Thus scattering phase shifts and related observables can be defined for $n \to \infty$. Indeed, a classical particle spends most time near a turning point defined by the energy $m\omega^2 r_0^2 = \hbar\omega(2n + \ell + 3/2)$, or

$$r_0 = \sqrt{\frac{\hbar}{m\omega}(2n + \ell + 3/2)}. \tag{32}$$

Thus for large n the wave function is represented by a peak at r_0, and the resulting form

$$|\phi_{n\ell}(r)|^2 \propto \frac{1}{\sqrt{r_0^2 - r^2}} \tag{33}$$

is sufficient to assure equivalence of the $n \to \infty$ limit to the asymptotic scattering limit.

We now transfer the problem into a discrete configuration space. The RGM solution (19) expressed in radial form (28) now needs to be matched with the asymptotic solution for the free-space Hamiltonian (30) so that similarly to Eq. (31) the asymptotic behavior is

$$\chi_n \simeq \alpha F_{n\ell} + \beta G_{n\ell}, \tag{34}$$

with $F_{n\ell}, G_{n\ell}$ representing regular and irregular solutions for the free-space Hamiltonian expanded in the HO basis; see Ref. [99]. The regular Coulomb function can be readily expanded,

$$F_{n\ell} = \int_0^\infty F_\ell(\eta, kr)\phi^*_{n\ell}(r)dr, \tag{35}$$

and inversely

$$F_\ell(\eta, kr) = \sum_{n=0}^{\infty} F_{n\ell}\phi_{n\ell}(r). \tag{36}$$

The coefficients $F_{n\ell}$ satisfy the infinite matrix equation

$$\sum_{n=0}^{\infty} \left(H^0_{mn} - E\delta_{mn}\right)F_{n\ell} = 0, \tag{37}$$

which reduces to a three term recursion in the case of the Laguerre basis or in the case of the HO basis for neutral particles.

The irregular function $G_\ell(\eta, kr)$ cannot be expanded in a similar fashion because the HO basis contains only regular functions. However, since we are interested in reproducing the asymptotic behavior, we can replace a true Coulomb function with any other function $\widetilde{G}_\ell(\eta, kr)$ regular at the origin, as long as asymptotically it coincides with $G_\ell(\eta, kr)$, thus

$$\begin{aligned} &\widetilde{G}_\ell(\eta, kr) = G_\ell(\eta, kr) \quad \text{for} \quad r \to \infty, \\ &\widetilde{G}_\ell(\eta, kr) \propto F_\ell(\eta, kr) \quad \text{for} \quad r \to 0. \end{aligned} \tag{38}$$

In order to minimally modify the irregular function near the origin the simplest strategy is to add a source term thus modifying Eq. (37) with an inhomogeneous term for $n = 0$,

$$\sum_{n'=0}^{\infty} \left(H^0_{nn'} - E\delta_{nn'}\right)G_{n'\ell} = g\delta_{n0}. \tag{39}$$

Following this change in the coordinate space the modified function

$$\widetilde{G}_\ell(\eta, kr) = \sum_{n=0}^{\infty} G_{n\ell}\phi_{n\ell}(r) \tag{40}$$

satisfies the following equation:

$$\left(-\frac{d^2}{dr^2} + \frac{2\eta k}{r} + \frac{\ell(\ell+1)}{r^2} - k^2\right)\widetilde{G}_\ell(\eta, kr) = \frac{2\mu g}{\hbar^2}\phi_{0\ell}(r). \tag{41}$$

An explicit form for $\widetilde{G}_\ell(r)$ can now be obtained via a standard Green's function, which is known analytically; see for example [95]. Taking into account the asymptotic limits (38), we arrive at the following full expression:

$$\begin{aligned} \widetilde{G}_\ell(\eta, kr) = \frac{2\mu g}{\hbar^2 k}\Bigg[&F_\ell(\eta, kr)\int_r^\infty G_\ell(\eta, kr')\phi_{0\ell}(r')dr' \\ &+ G_\ell(\eta, kr)\int_0^r F_\ell(\eta, kr')\phi_{0\ell}(r')dr'\Bigg], \end{aligned} \tag{42}$$

and by matching at $r \to \infty$,

$$g = \frac{\hbar^2 k}{2\mu F_{0\ell}}. \tag{43}$$

This strategy provides a formal definition for coefficients $G_{n\ell}$ in expansion (34),

$$G_{n\ell} = \int_0^\infty \phi^*_{n\ell}(r)\widetilde{G}_\ell(r)dr. \tag{44}$$

The expansion coefficients $F_{n\ell}$ and $G_{n\ell}$ are known analytically for the limit of neutral particles ($\eta = 0$) [40,57,98]. In the absence of Coulomb interaction, H^0 contains only a kinetic energy term which leads to a tridiagonal matrix $H_{nn'}$, as the kinetic energy operator can at most increase the number of oscillator quanta by 2 and matrix equations (37) and (39) represent recurrence relations.

The truncation of the basis at some value n_0 gives rise to an internal and an external space, labeled here as $\mathcal{P}$ and $\mathcal{Q}$ respectively. The space $\mathcal{P}$ is of dimension $n_0 + 1$ containing all basis functions with $0 \leqslant n \leqslant n_0$. On the other hand, the space $\mathcal{Q}$, dubbed the external space, contains matrix elements of the free Hamiltonian. Thus, we apply here an approximation that amounts to an assumption that our Hamiltonian and Norm kernels in Eq. (21) are a range limited in configuration space to $n \leqslant n_0$. Outside, in the $\mathcal{Q}$ space, for $n > n_0$, the wave function has an asymptotic form (34).

The $\mathcal{P}$ space components can be obtained using a propagator

$$\mathcal{G}_{\mathcal{P}\mathcal{P}} = \frac{1}{E\mathcal{N}_{\mathcal{P}\mathcal{P}} - \mathcal{H}_{\mathcal{P}\mathcal{P}}}, \tag{45}$$

as

$$\chi_{\mathcal{P}} = \mathcal{G}_{\mathcal{P}\mathcal{P}}H^0_{\mathcal{P}\mathcal{Q}}\chi_{\mathcal{Q}}, \tag{46}$$

where components in the $\mathcal{Q}$ space have the asymptotic form defined in Eq. (34). The propagator in the relatively small space $\mathcal{P}$ is easily calculated numerically. The matching between internal and external space is set at $n = n_0$ by making

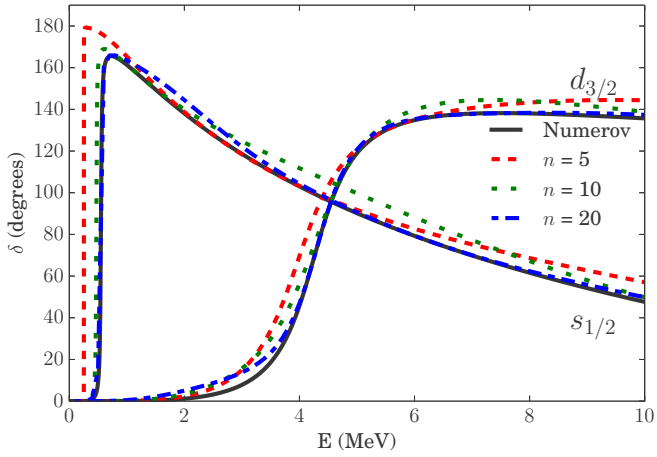

FIG. 9. $s_{1/2}$ and $d_{3/2}$ phase shifts for the Woods-Saxon potential (see text for parameters) compared to the ones obtained with the Numerov method.

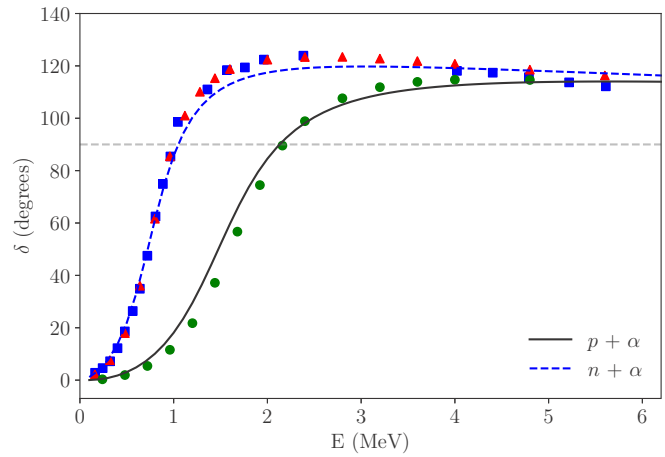

FIG. 10. $n + \alpha$ and $p + \alpha$ phase shifts in the $p_{3/2}$ channel. Experimental points are taken from [102] (blue squares) and [103] (red triangles) for $n + \alpha$, and from [104] (green circles) for $p + \alpha$ scattering.

the assumption that

$$\chi_{n_0} = \alpha F_{n_0\ell} + \beta G_{n_0\ell}. \tag{47}$$

Equation (46) and matching assumption (47) lead to a standard HORSE method, where if H^0 contains only kinetic energy then there is only one off-diagonal matrix element $H^0_{\mathcal{PQ}}$ that connects the spaces, namely $H^0_{n_0 n_0+1}$. Therefore

$$\alpha F_{n_0\ell} + \beta G_{n_0\ell} = \mathcal{G}_{n_0 n_0} H^0_{n_0 n_0+1}\big(\alpha F_{n_0+1\ell} + \beta G_{n_0+1\ell}\big), \tag{48}$$

which allows us to determine the β/α ratio and the phase shift.

The Coulomb component in the free-space Hamiltonian H^0 does not allow for a simple form of Eq. (48); the $H^0_{\mathcal{PQ}}$ is no longer given by a single matrix element, instead all states in the external space become coupled. Carrying out the summations becomes impractical, thus we suggest a different strategy. Using free space solutions (37) and (39) we rewrite

$$H^0_{\mathcal{PQ}}\chi_{\mathcal{Q}} = E\chi_{\mathcal{P}} - H^0_{\mathcal{PP}}\chi_{\mathcal{P}} + g\beta\delta_{n0}, \tag{49}$$

where we include a source term of Eq. (39). The phase shift $\tan\delta_\ell = \beta/\alpha$ is then obtained using the finite sums and quantities evaluated completely within the $\mathcal{P}$ space; the explicit equation is as follows:

$$\frac{\beta}{\alpha} = \frac{-F_{n_0\ell} + \sum_{n=0}^{n_0}\mathcal{G}_{n_0 n}\big(EF_{n\ell} - \sum_{n'=0}^{n_0} H^0_{nn'}F_{n'\ell}\big)}{G_{n_0\ell} - \sum_{n=0}^{n_0}\mathcal{G}_{n_0 n}\big(EG_{n\ell} + g\delta_{n0} - \sum_{n'=0}^{n_0} H^0_{nn'}G_{n'\ell}\big)}. \tag{50}$$

In summary, the expression of Eq. (50) is the main result here. It allows for a study of reactions with cluster channels involving Coulomb interactions avoiding exterior space summations that could be unstable or/and poorly convergent.

In Fig. 9 we show a proof-of-principle calculation using a Woods-Saxon potential. Since for neutral particles the HORSE method, tested in Ref. [98], is recovered exactly, we limit our testing to proton resonances in the potential. The parameters used here follow parametrization [100] for the central potential $V_0 = -48.25$ MeV, $R_0 = 3.239\,81$ fm; for the spin-orbit potential $V_{ls} = 22.8386$ MeV, $R_{ls} = 3.084\,25$ fm; and for both potentials the diffuseness $\alpha_0 = \alpha_{ls} = 0.644\,174$ fm; the Coulomb potential is described by that of a hard uniformly charged sphere of radius $R_C = 3.239\,81$. This choice of parameters, along with the reduced mass $\mu = 882.671\,\text{MeV}/c^2$, approximates proton resonances in ^{17}F that carry the single-particle quantum numbers $s_{1/2}$, $d_{3/2}$, and $d_{5/2}$. We choose two representative cases to show that the $d_{3/2}$ resonance with energy 4.48 MeV and width 0.82 MeV is relatively broad, while the $s_{1/2}$ at energy 0.55 MeV and width of 25 keV is narrow. In Fig. 9 the convergence pattern of the phase shifts with increasing size of the $\mathcal{P}$ space is shown. The basis used is the HO basis with $\hbar\omega = 25$ MeV, and therefore the characteristic oscillator length is about 1.76 fm. Following Eq. (32) we can associate $n = 3$, 10, and 20 with $r_0 = 4.8$, 8.2, and 11.4 fm, respectively. Comparison of r_0 with the radius and diffuseness, quoted earlier, explains the quality of the agreement in Fig. 9 between this method and the exact result obtained using the standard numerical integration technique (Numerov method).

Next we consider both neutrons and protons scattering off an α particle. The $p + \alpha$ and $n + \alpha$ channels are constructed with the α particle described by a s^4 configuration. Similar to the discussion in Sec. III D, the basis channels describe a nucleon-α system in a relative state with HO wave function enumerated by the number of nodes. The norm of the channels, similar to Eq. (C2), follows a simple analytic expression $\mathcal{N}_{nn'} = [1 - (-1/4)^{2n+\ell}]\delta_{nn'}$. Due to the s^4 approximation, each channel has a different total number of HO quanta making the channels orthogonal. We use the JISP16 interaction [101] and truncate the basis at $N = 2n + \ell = 6$. This value of $\hbar\omega = 25$ MeV corresponds to $r_0 = 3.5$ fm for this truncation of the basis channels which is expected to be sufficient to describe an alpha-nucleon potential. The results, shown in Fig. 10, show a good agreement with the experimentally observed ones provided that the reaction kinematics is properly satisfied. Here the interior wave function from the RGM solution is matched to exterior asymptotic states of proper,

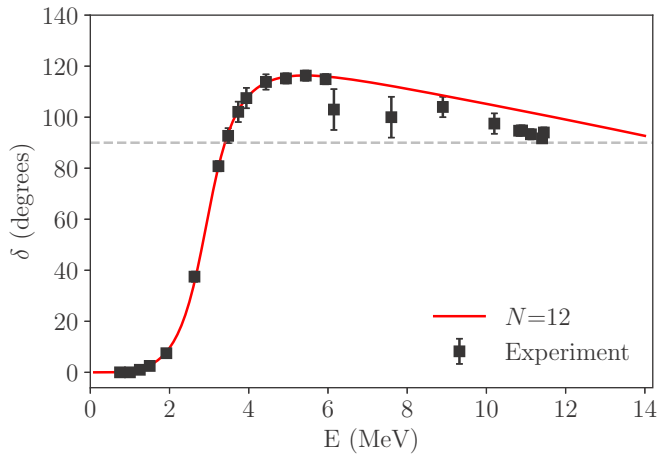

FIG. 11. The $\alpha + \alpha$ phase shifts in the $\ell = 2$ channel. Experimental data are taken from [105]. The solid line shows the result of the calculation including up to $N = 12$ quanta in the relative motion wave function, while the dashed shows a truncated space with a single channel.

experimentally known, energy. This is a standard procedure since it is unrealistic to expect the current microscopic models based on fundamental nucleon-nucleon interactions to provide energies with a kilovolt level of precision required to properly describe sensitive reaction processes such as tunneling over the Coulomb barrier.

As a final application, we evaluate phase shifts for $\alpha + \alpha$ scattering with the α particles approximated as s^4. This application combines our structural study in Sec. III D with the scattering approach formulated in Sec. IV, and goes beyond a trivial bound-state-type matching discussed in Table V. Here, again the experimental threshold energies have been used. The $\ell = 2$ phase shifts are shown in Fig. 11. In order to make a comparison with older calculations more transparent the same Hamiltonian and Norm kernel matrix elements as in Ref. [29] are used. The agreement with experiment, once the threshold is set to the experimental value, is very good.

V. CONCLUSIONS

Nuclear clustering and emergence of clustering degrees of freedom in atomic nuclei is an important topic of modern nuclear physics. In this work we continue developments reported in Ref. [29] and put forward a new configuration-interaction-based method that aims to further unify different strategies and techniques, as well as structure and reactions aiming at questions of clustering in atomic nuclei. We provide an extensive discussion with multiple examples showing features and advantages of the approach.

The method is built upon extensive experience within the traditional shell model and its algebraic limits, thus approximations such as limiting valence space or assuming a trivial structure for an α particle reduce our approach to well-studied limits. This reduction not only provides for a good test and alternative methods for numerical calculation of algebraic cluster coefficients, but it also assesses the quality and limits of validity of the previously used simplified strategies.

The method easily bridges between the traditional and more modern microscopic nuclear many-body techniques based on HO Slater determinant basis expansions, thus allowing us to connect broad phenomenological experience of the traditional nuclear shell model with yet poorly understood questions of clustering. Being built on a powerful center-of-mass boosting procedure, utilizing cluster configurations and modern programming techniques, our approach represents an advancement in many-body methods and configuration interaction approaches. We extensively explore the boosting method introduced in Ref. [29] both in the traditional shell model phenomenological regime and within the NCSM.

We demonstrate the new approach using *sd* shell nuclei, where previous theoretical studies and availability of experimental data allow for quantitative comparisons. Special attention is devoted to ^{20}Ne due to its pronounced cluster structure. Detailed experimental information on alpha clustering in excited states provides valuable data allowing us to discuss in detail the form of the effective α-cluster channel.

Similarly, in ^{21}Ne an extra nucleon distorts the $^{16}\mathrm{O} + \alpha$ motion and leads to orbital angular momentum mixing which offers a strategy for testing molecularlike cluster motion and the ability of our model to describe it. Our results are in good agreement with the existing experimental data and we provide comprehensive information on channel mixing matrix elements in RGM equations that can be tested in future experiments.

As has been experimentally observed and discussed by numerous authors, clustering appears to be a near-threshold phenomenon where many-body structure and reactions are inevitably entangled. This work builds yet another bridge between reaction dynamics and many-body structure. While maintaining full antisymmetry between nucleons and translational invariance, we build cluster channels and study their static structural properties. The same channels are then used to study reactions and reaction observables. A method for dealing with the Coulomb problem within the harmonic oscillator representation of scattering equations has been further developed for this purpose. Within this extension we expect to further probe the role of continuum degrees of freedom in the emergence of clustering.

We have performed an extensive study of ^{8}Be, which is a standard benchmark in clustering methods. In our work we use the ^{8}Be example to show the full structure-reaction path which includes obtaining a shell model solution and spectrum, constructing the cluster channels, structural spectroscopic factors, obtaining decay widths in the perturbative limit, and finally a study of ^{8}Be as $\alpha + \alpha$ resonances. All of these studies utilize the same nuclear Hamiltonian and emerge within the same overall framework.

One interesting indirect finding of this work is that clustering appears to be adequately described within relatively small configuration spaces; this result raises immediate questions that should be explored in the future.

ACKNOWLEDGMENTS

We are grateful to T. Dytrych, V. Z. Goldberg, S. Quaglioni, G. V. Rogachev, A. Shirokov, and Yu. Tchuvil'sky

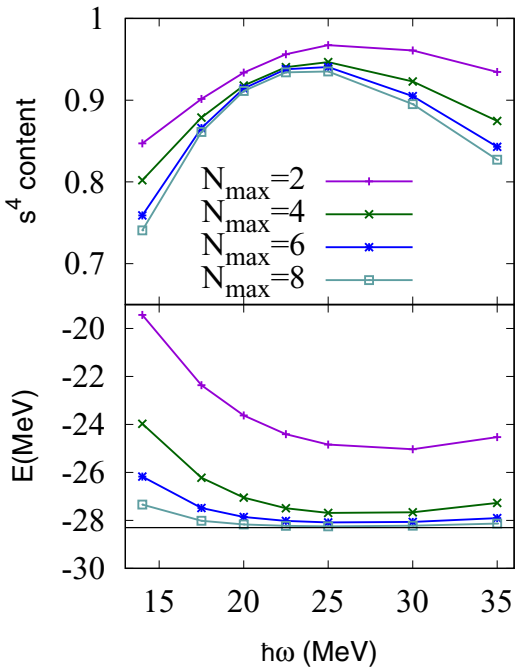

FIG. 12. NCSM calculations with JISP16 interaction showing the ground state energy of ^{4}He as a function of $\hbar\omega$ values (bottom) and the fraction of s^4 component of the ^{4}He wave function (top). Curves correspond to different truncations $N_{\max}$.

for their help and comments related to this work. This material is based upon work supported by the US Department of Energy Office of Science, Office of Nuclear Physics under Award No. DE-SC0009883. This article was prepared in part by Lawrence Livermore National Laboratory under Contract No. DE-AC52-07NA27344.

APPENDIX A: STRUCTURE OF c.m.-BOOSTED STATES

In this Appendix we comment on the structure of the c.m.-boosted states and connection to the SU(3) based models that have been widely used in the literature [34,35,52,82]. To make the connection, we limit this discussion to c.m.-boosted wave functions of α particles. As shown in Fig. 12, the ground state of an α particle is predominately a state of four nucleons fully occupying the lowest oscillator shell; we refer to this arrangement as an s^4 configuration. The weight of this component is over 90% for a rather broad range, approximately between 20 and 30 MeV, of oscillator frequencies $\hbar\omega$.

By making an approximation, the quality of which thus depends on $\hbar\omega$, that the α particle has a simplified s^4 structure or equivalently it is computed with an $N_{\max} = 0$ truncation of the basis, we arrive at the algebraic limit [34,35,82]. For clusters that have no intrinsic oscillator excitation quanta N'=0 the wave function $\Psi_{n\ell m}$ has all quanta exclusively in the c.m. part; the spatial part remains fully symmetric with respect to permutations, moreover it is clear that with respect to SU(3) symmetry related to spatial directions only $(\lambda, \mu) = (N, 0)$ irreducible representations contribute. Thus, in the algebraic limit, we can expand

$$\Psi_{n\ell m} = \sum_{\eta} X_N^{\eta}\, \Phi^{\eta}_{(N,0):\ell m}. \tag{A1}$$

over all partitions η where A nucleons are partitioned over oscillator shells $A = \sum_i \alpha_i$ in such a way that the combined number of quanta is $N = 2n + \ell = \sum_i \alpha_i N_i$. The coefficients in expansion (A1), commonly known as cluster coefficients [35,52,82], are known analytically,

$$X_N^{\eta} = \sqrt{\frac{1}{4^N}\,\frac{N!}{\prod_i (N_i!)^{\alpha_i}}\,\frac{4!}{\prod_i \alpha_i!}}. \tag{A2}$$

The wave function $\Phi^{\eta}_{(N,0):\ell m}$ is the wave function of the $(N, 0)$ SU(3) symmetry and full permutational symmetry for this partition, which is unique. Most shell model studies of α clustering in nuclei [34,35,52,106] rely on expansion (A1). In our work we built wave function (6) via sequential c.m.-boost operations resulting in a much simpler procedure that works for any cluster of any structure. In Table VII we illustrate weights of select configurations for a boosted state Ψ_{400} for α particle. For the left column, the α particle is approximated by an s^4 closed shell wave function, while for the right column $\Psi = \Psi_{000}$ is taken from a realistic NCSM calculation with $N_{\max} = 4$. The data in the left column reproduce the cluster coefficients squared (A2); in this algebraic limit only configurations with $N = 8$ quanta are allowed and thus configurations such as $(p)(sd)(pf)(sdg)$ that has $N = 10$ only become possible when a more realistic α particle structure is used.

TABLE VII. Select configuration content of NCSM wave functions for ^{4}He with $\hbar\omega = 20$ MeV boosted to a c.m. boosted state with $n = 4$ and $\ell = 0$.

Configuration	$N_{\max} = 0$	$N_{\max} = 4$
$(sd)^4$	0.038	0.035
$(p)(sd)^2(pf)$	0.308	0.282
$(p)^2(pf)^2$	0.103	0.094
$(p)^2(sd)(sdg)$	0.154	0.141
$(p)(sd)(sdg)(pfh)$	0.000	0.005
$(p)(sd)(pf)(sdg)$	0.000	0.009

Another perspective on the c.m.-boosted state is provided by Fig. 13 where nucleon occupancy of various HO shells is shown for different boosted α-particle states where c.m. component of the wave function has different number of nodes n. This figure gives a microscopic illustration of cluster separation both in configuration and in coordinate space; we will return to this point in Sec. IV [see Eq. (32) in particular], and highlights the limitations of restricted valence spaces commonly encountered in the traditional shell model valence spaces, and could potentially explain disagreements with experiment observed in Refs. [15,66].

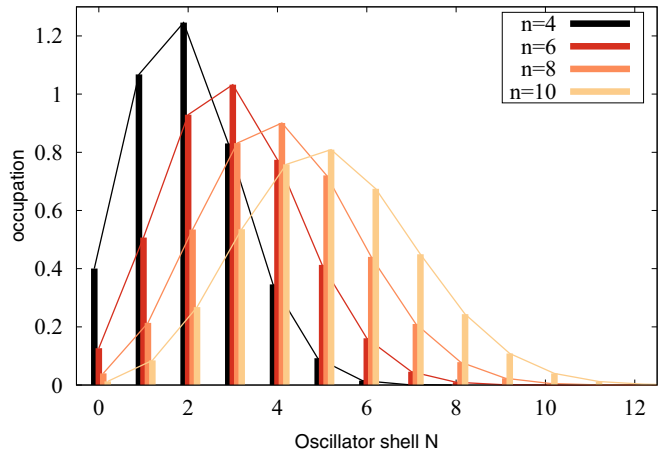

FIG. 13. Distribution of nucleon occupancies normalized to by total $A = 4$ over HO shells for the c.m.-boosted wave function $\Psi_{n\ell m}$ where $\ell = 0$, $m = 0$ and Ψ is taken as s^4. Different lines correspond to $n = 4, 6, 8$ and 10, as labeled.

APPENDIX B: STRUCTURAL SPECTROSCOPIC CHARACTERISTICS

The basis channels are naturally mixed. The interaction Hamiltonian through the RGM procedure discussed in Sec. II D determines the asymptotic reaction channels and reaction properties. However, it is instructive to discuss and illustrate the properties of the basis cluster channels which is done in this part of the Appendix. In a number of traditional shell model studies the valence space is restricted to a single oscillator shell. Many clustering studies have been done in the p shell [63,107] and sd shell [34,52] where configuration space allows only for a single basis channel to contribute and hence any kind of mixing is not possible, therefore the basis channel is approximately equated to a reaction channel. Let us remind and connect our discussion to some well-established aspects of clustering using a trivial example discussed in Table VIII where the ground state of ^{16}O is taken to cluster into the ground state of ^{12}C and an α particle. The ground states for ^{16}O and an α particle are taken to be closed core; we show results for three choices of wave functions that approximate the ground state of ^{12}C: closed subshell, $(p_{3/2})^8$ configuration, and an algebraic SU(3) $(\lambda, \mu) = (0, 4)$ configuration. The table illustrates workings of Eq. (17) by

TABLE VIII. Example showing channel construction for $^{12}\mathrm{C} + \alpha$.

$\{n_1, \ell_1\}$	$\{n_2, \ell_2\}$	$\mathcal{M}^{2000;0}_{n_1\ell_1 n_2\ell_2}$	$(0p_{3/2})^8$	SU(3)
0,0	2,0	$\frac{9}{16} \approx 0.563$	0.0761	$\sqrt{3/32}$
0,1	1,1	$-\frac{3\sqrt{3}}{8} \approx -0.650$	−0.0878	$-1/\sqrt{8}$
0,2	0,2	$\sqrt{\frac{3}{32}} \approx 0.306$	0.0414	$1/\sqrt{32}$
1,0	1,0	$\sqrt{\frac{15}{128}} \approx 0.342$	0.0463	$\sqrt{5}/12$
1,1	0,1	$-\frac{\sqrt{3}}{8} \approx -0.217$	−0.0293	$-1/\sqrt{72}$
2,0	0,0	$\frac{1}{16} \approx 0.063$	0.0085	$1/\sqrt{864}$

showing an overlap with the parent ^{16}O,

$$\langle \Psi^{(^{16}\mathrm{O})} | \Phi_{200} \rangle = \sum_{n_1\ell_1 n_2\ell_2} \mathcal{M}^{2000;0}_{n_1\ell_1 n_2\ell_2} \langle \Psi^{(^{16}\mathrm{O})} | \left[\Psi^{(^{12}\mathrm{C})\dagger}_{n_1\ell_1 m_1} \times \Psi^{(\alpha)\dagger}_{n_2\ell_2 m_2} \right]_{00} | 0 \rangle. \quad \text{(B1)}$$

The only possible channel in the p shell is with $N_{\mathrm{rel}} = 4$; all nuclear states carry no spin making any angular momentum recoupling trivial. The only contributing $^{12}\mathrm{C} + \alpha$ relative angular momentum $\ell = 0$ sets the number of nodes in the relative wave function to $n = 2$. A restriction of this type is commonly known as Wildermuth condition [108,109], and it is based on the number of quanta and Pauli exclusion principle. In Table VIII for each set of possible n_1, ℓ_1, n_2, ℓ_2 where the index 1 denotes c.m.-boosted ^{12}C and the index 2 stands for α we show oscillator bracket $\mathcal{M}$ followed by the overlap $\langle \Psi^{(^{16}\mathrm{O})} | [\Psi^{(^{12}\mathrm{C})\dagger}_{n_1\ell_1 m_1} \Psi^{(\alpha)\dagger}_{n_2\ell_2 m_2}]_{00} | 0 \rangle$. Thus, the last two columns labeled $(0p_{3/2})^8$ and SU(3) correspond to this overlap assuming ^{12}C wave function $\Psi^{(^{12}\mathrm{C})}$ being filled, $0p_{3/2}$ subshell, and $(\lambda, \mu) = (0, 4)$ SU(3) configuration, respectively. The SU(3) limit is known analytically and provides a valuable numerical test for our method. With ^{12}C being heavier than an α the c.m. effect of recoil is visible; the largest oscillator bracket comes when α is boosted to $n_2 = n = 2$ and $\ell_2 = \ell = 0$. This oscillator bracket in the first row would be equal to unity if ^{12}C were infinitely heavier than an α.

Until recently, the absolute values squared of overlaps such as (B1) were interpreted as spectroscopic factors (SFs) [35,52,82,110–113],

$$S_{n,\ell} \equiv |\langle \Psi^{(A)} | \Phi_{n\ell} \rangle|^2. \quad \text{(B2)}$$

In cases with multiple contributing basis channels n the total SF is assumed to be a simple sum,

$$S_\ell = \sum_n S_{n,\ell}. \quad \text{(B3)}$$

The SFs are translationally invariant since both sides of the overlap (B2) contain an overall c.m. wave function in its ground state (nonspurious state). In fact, given that the parent state $\Psi^{(A)}$ is nonspurious this state projects out the nonspurious c.m. component in an overlap. With orthogonality of the recoupling brackets we can invert a product

$$\left| \Psi_{n_1\ell_1} \Psi_{n_2\ell_2} \right\rangle = \sum_{\substack{n_{cm}\ell_{cm} \\ n\ell}} \mathcal{M}^{n\ell n_{\mathrm{cm}}\ell_{\mathrm{cm}}}_{n_1\ell_1 n_2\ell_2} \left| \phi_{n_{\mathrm{cm}}\ell_{\mathrm{cm}}}(\mathbf{R}) \phi_{n\ell}(\boldsymbol{\rho}) \Psi'^{(1)} \Psi'^{(2)} \right\rangle, \quad \text{(B4)}$$

where both sides of the equation are assumed to be coupled to proper channel quantum numbers which we suppress and therefore magnetic quantum numbers are not shown. An overlap of (B4) with a nonspurious state gives

$$\mathcal{M}^{n\ell 00;\ell}_{n_1\ell_1 n_2\ell_2} \langle \Psi^{(A)} | \Phi_{n\ell} \rangle = \left\langle \Psi^{(A)} \middle| \left[\Psi^\dagger_{n_1\ell_1 m_1} \Psi^\dagger_{n_2\ell_2 m_2} \right]_\ell \right\rangle. \quad \text{(B5)}$$

From here it follows that the amplitude for the traditional spectroscopic factor could be found from any row of Table VIII; the overlaps in either of the last two columns divided by the Talmi-Moshinsky-Smirnov coefficient in the fifth column is always the same, giving the spectroscopic

amplitude. Therefore, it is convenient to take the row with the largest oscillator bracket, which as discussed earlier amounts to taking the heavier fragment with nonspurious c.m. motion, as it comes directly from the SM, and only boosting the lighter fragment,

$$\langle \Psi^{(A)} | \Phi_{n\ell} \rangle = R \, \langle \Psi^{(A)} | \big[\Psi^{\dagger} \times \Psi^{\dagger}_{n\ell m} \big]_{\ell} | 0 \rangle. \tag{B6}$$

The recoil coefficient here is

$$R \equiv \left(\mathcal{M}^{n\ell 00;\ell}_{00 n\ell} \right)^{-1} = (-1)^{N_{\rm rel}} \left(\frac{A}{A_1} \right)^{N_{\rm rel}/2}, \tag{B7}$$

where A/A_1 represents the mass ratio and $N_{\rm rel} = 2n + \ell$.

The traditional spectroscopic factors discussed here for clusters can be seen as generalizing the single-particle spectroscopic factors used in nearly all shell model studies; see for example Ref. [114]. The c.m.-boosting procedure applied for a single nucleon is equivalent to placing the nucleon being emitted on the HO orbit with the correct quantum number of the channel. Spin, parity, and limitations of the valance space in most practical cases lead to just a single choice for the single-particle state from which a nucleon can be removed, i.e., radial quantum number n. Due to small nucleon mass the recoil is commonly ignored, setting $R \approx 1$, however more exact recoil-corrected reaction studies have been done [115].

It is possible to obtain translationally invariant matrix elements of operators, assuming those are translationally invariant as well; see also [62]. Keeping the heavier system 2 in nonspurious state $n_2 = 0$ and $\ell_2 = 0$ we can make a list of nontranslationally invariant products with quantum numbers identical to those of the channels. Using Eq. (B4) we obtain a set of equations

$$\begin{aligned} &\left\langle \Psi^{(1)}_{n_1\ell_1} \Psi^{(2)}_{00} \middle| \mathcal{O} \middle| \Psi^{(1)}_{n'_1\ell'_1} \Psi^{(2)}_{00} \right\rangle \\ &\quad = \sum_{\substack{n_{cm}\ell_{cm} \\ n_1\ell_1 n'\ell'}} \mathcal{M}^{n\ell n_{\rm cm}\ell_{\rm cm}}_{n_1\ell_1 00} \mathcal{M}^{n'\ell' n_{\rm cm}\ell_{\rm cm}}_{n'_1\ell'_1 00} \langle \Phi_{n\ell} | \mathcal{O} | \Phi_{n'\ell'} \rangle, \end{aligned} \tag{B8}$$

which can be solved to obtain translationally invariant matrix elements $\langle \Phi_{n\ell} | \mathcal{O} | \Phi_{n'\ell'} \rangle$ of any translationally invariant operator $\mathcal{O}$ for all basis channels $\Phi_{n\ell}$. The approach can be generalized to include nonelastic channels.

The spectroscopic factors provide valuable structural information and are very useful in experimental studies, however, one should keep in mind that their applicability is limited to weak continuum coupling. For reaction studies full channel wave functions such as those in Eqs. (17) and (18) are necessary; and similar to shell model studies that involve single-particle continuum [18,116,117] the reaction channels introduce structural changes into decaying states.

APPENDIX C: CHANNEL ORTHOGONALITY AND NORMALIZATION

In this Appendix we discuss nonorthogonality of the basis channels and the norm kernel. In Table IX, see also [29], we provide some examples that show spectroscopic amplitudes and channel normalizations for select cases. The first two lines summarize the $n = 2$, $\ell = 0$ channel basis state discussed in Table VIII. Other examples include basis channels for ^{8}Be which are necessary for RGM study in Sec. III D and for $\alpha + \alpha$ scattering discussed in Sec. IV, as well as select multi-α cluster basis channels with minimal number of quanta in relative motion for ^{12}C and ^{16}O. Because of the simple structure, most of the results presented in Table VIII are known analytically; we emphasize this by retaining those exact expressions.

TABLE IX. Absolute values of spectroscopic amplitudes and channel norms for various types of parent states and basis channels; see also Ref. [29]. All channels here have $\ell = 0$ and the number of quanta in relative motion of the two fragments is denoted by $N_{\rm rel} = 2n + \ell$. For each nucleus square brackets indicate the structure used for the corresponding fragment which could include spectroscopic notation, a pair of SU(3) quantum numbers, or $N_{\rm max}$ as a single integer. For the latter cases NCSM calculations with JISP16 were used with $\hbar\omega = 20$ MeV.

Parent	Channel	$N_{\rm rel}$	$\lvert\langle\Psi\lvert\Phi_{n\ell}\rangle\rvert$	$\langle\Phi_{n\ell}\lvert\Phi_{n\ell}\rangle$
^{16}O[0]	^{12}C[(0, 4)] + α[0]	4	$\sqrt{8/27}$	8/27
^{16}O[0]	^{12}C[$p^8_{3/2}$] + α[0]	4	0.135	0.018
^{16}O[0]	^{12}C[$p^8_{3/2}$] + α[4]	4	0.130	0.017
^{8}Be[(4, 0)]	α[0] + α[0]	4	$\sqrt{3/2}$	3/2
^{8}Be[0]	α[0] + α[0]	4	1.160	3/2
^{8}Be[4]	α[0] + α[0]	4	0.984	3/2
^{8}Be[4]	α[0] + α[0]	6	0.644	15/8
^{8}Be[4]	α[2] + α[2]	4	0.981	1.492
^{12}C[$p^8_{3/2}$]	α[0] + α[0] + α[0]	8	1/4	81/80
^{16}O[0]	$(\alpha[0])^4$	12	$\sqrt{3/10}$	3/10

For the basis set of channel wave functions $\Phi_{n\ell}$ labeled by generalized index n we introduce the norm kernel

$$\mathcal{N}^{(\ell)}_{nn'} = \langle \Phi_{n\ell} | \Phi_{n'\ell} \rangle. \tag{C1}$$

The last column in Table IX shows examples of diagonal matrix elements of the norm kernel. The norm kernel is exclusively a structural characteristic reflecting properties of cluster configurations. Only indirectly, through the structure of clusters, it is tied to the underlying microscopic nucleon-nucleon interaction. In the cases where specific HO structure can be assumed, such as closed shell nuclei, the norm kernel is universal. For clusters whose structure is described within a single oscillator shell ($N_{\rm max} = 0$ approximation) the total number of oscillator quanta within each basis channel is fixed which enforces an additional orthogonality. For example for $\alpha[0] + \alpha[0]$ the norm kernel is diagonal and known analytically [118],

$$\mathcal{N}^{(\ell)}_{nn'} = \delta_{nn'} 2(1 - 2^{2-2n-\ell}), \tag{C2}$$

where to satisfy Pauli exclusion principle $2n + \ell = N_{\rm rel} \geqslant 4$, and bosonlike permutational symmetry of two α's requires ℓ to be even. If any of these conditions is not fulfilled, then $\mathcal{N}^{(\ell)}_{nn'} = 0$. These rules are fully reproduced in our numerical studies. Asymptotically for $n \to \infty$ the $\mathcal{N}^{(\ell)}_{nn} \simeq 2$ as it would be expected for a state of two identical bosons constructed following Eq. (17).

Unlike for electromagnetic or single-particle channels [116], where it is straightforward to normalize reaction channels and thus establish the corresponding sum rules, the situation with composite objects such as clusters is more difficult.

The true channels have to be properly normalized asymptotically, which is done within the RGM approach. However, within the traditional shell model with the valence space where only very few basis channels are possible, Fliessbach and others have argued in Refs. [119–121] for the orthogonality conditions model (OCM). The OCM spectroscopic factors which have been widely used recently have shown to be a significant improvement over the traditional SF in Eq. (B3); see Ref. [52]. In the modified approach the set of basis reaction channels is orthonormalized using the norm kernel leading to a set of channel vectors labeled with index ν,

$$\left|\Psi_{\nu}^{(\ell\text{OCM})}\right\rangle = \sum_{n}\left(\frac{1}{\sqrt{\mathcal{N}^{(\ell)}}}\right)_{\nu n}|\Phi_{n\ell}\rangle. \tag{C3}$$

Here $(1/\sqrt{\mathcal{N}^{(\ell)}})_{\nu n}$ is a matrix element of the norm kernel matrix raised to the power of $-1/2$ which is typically achieved via diagonalization. The index ν by itself does not have any particular physical meaning but the part of the full parent state wave function spanned by the orthonormalized set of vectors ν defines the spectroscopic factor:

$$S_{\ell}^{(\text{OCM})} \equiv \sum_{\nu}\left|\left\langle\Psi^{(A)}\middle|\Psi_{\nu}^{(\ell\text{OCM})}\right\rangle\right|^2. \tag{C4}$$

The OCM SFs ($S_{\ell}^{(\text{OCM})}$) are normalized so that the sum of all reduced transition probabilities from all initial states into a particular asymptotic channel equals the dimensionality of the space ν, equivalently to the number of basis channels n; this does not include different magnetic substates of the asymptotic channel [52].

[1] National Research Council, *Nuclear Physics: Exploring the Heart of Matter* (The National Academies Press, Washington, DC, 2013).
[2] A. Aprahamian *et al.*, *Reaching for the Horizon: The 2015 Long Range Plan for Nuclear Science* (2015), https://science.osti.gov/-/media/np/nsac/pdf/2015LRP/2015_LRPNS_091815.pdf.
[3] G. Gamow, Proc. R. Soc. London, Ser. A **126**, 632 (1930).
[4] L. R. Hafstad and E. Teller, Phys. Rev. **54**, 681 (1938).
[5] J. Blatt and V. Weisskopf, *Theoretical Nuclear Physics*, Dover Books on Physics (Dover, Mineola, New York, 2012).
[6] M. Freer, Rep. Prog. Phys. **70**, 2149 (2007).
[7] Y. Kanada-En'yo, M. Kimura, and A. Ono, Prog. Theor. Exp. Phys. **2012**, 01A202 (2012).
[8] W. von Oertzen, Phys. Scr. **2000**, 83 (2000).
[9] W. von Oertzen, M. Freer, and Y. Kanada-En'yo, Phys. Rep. **432**, 43 (2006).
[10] R. Bijker and F. Iachello, Phys. Rev. C **61**, 067305 (2000).
[11] R. Bijker and F. Iachello, Phys. Rev. Lett. **112**, 152501 (2014).
[12] N. Curtis, N. M. Clarke, B. R. Fulton, S. J. Hall, M. J. Leddy, A. S. J. Murphy, J. S. Pople, R. P. Ward, W. N. Catford, G. J. Gyapong *et al.*, Phys. Rev. C **51**, 1554 (1995).
[13] N. Curtis, A. S. J. Murphy, N. M. Clarke, M. Freer, B. R. Fulton, S. J. Hall, M. J. Leddy, J. S. Pople, G. Tungate, R. P. Ward *et al.*, Phys. Rev. C **53**, 1804 (1996).
[14] K. Ikeda, N. Takigawa, and H. Horiuchi, Prog. Theor. Phys. Suppl. **E68**, 464 (1968).
[15] M. L. Avila, G. V. Rogachev, V. Z. Goldberg, E. D. Johnson, K. W. Kemper, Y. M. Tchuvil'sky, and A. S. Volya, Phys. Rev. C **90**, 024327 (2014).
[16] A. N. Kuchera, G. V. Rogachev, V. Z. Goldberg, E. D. Johnson, S. Cherubini, M. Gulino, M. La Cognata, L. Lamia, S. Romano, L. E. Miller, R. G. Pizzone, G. G. Rapisarda, M. L. Sergi, C. Spitaleri, R. E. Tribble, W. H. Trzaska, and A. Tumino, Phys. Rev. C **84**, 054615 (2011).
[17] A. N. Kuchera, Ph.D. thesis, The Florida State University, 2013, http://purl.flvc.org/fsu/fd/FSU_migr_etd-8585.
[18] J. Okołowicz, M. Płoszajczak, and I. Rotter, Phys. Rep. **374**, 271 (2003).
[19] N. Auerbach and V. Zelevinsky, Rep. Prog. Phys. **74**, 106301 (2011).
[20] A. Volya and V. Zelevinsky, Phys. At. Nucl. **77**, 969 (2014).
[21] K. Kravvaris and A. Volya, in *Nuclei and Mesoscopic Physics 2017*, edited by P. Danielewicz and V. Zelevinsky, AIP Conf. Proc. No. 1912 (AIP, Melville, NY, 2017), p. 020010.
[22] D. N. F. Dunbar, R. E. Pixley, W. A. Wenzel, and W. Whaling, Phys. Rev. **92**, 649 (1953).
[23] F. Hoyle, Astrophys. J., Suppl. Ser. **1**, 121 (1954).
[24] M. Freer, A. H. Wuosmaa, R. R. Betts, D. J. Henderson, P. Wilt, R. W. Zurmühle, D. P. Balamuth, S. Barrow, D. Benton, Q. Li *et al.*, Phys. Rev. C **49**, R1751 (1994).
[25] A. Raduta, B. Borderie, E. Geraci, N. L. Neindre, P. Napolitani, M. Rivet, R. Alba, F. Amorini, G. Cardella, M. Chatterjee *et al.*, Phys. Lett. B **705**, 65 (2011).
[26] M. Itoh, S. Ando, T. Aoki, H. Arikawa, S. Ezure, K. Harada, T. Hayamizu, T. Inoue, T. Ishikawa, K. Kato *et al.*, Phys. Rev. Lett. **113**, 102501 (2014).
[27] R. Smith, T. Kokalova, C. Wheldon, J. E. Bishop, M. Freer, N. Curtis, and D. J. Parker, Phys. Rev. Lett. **119**, 132502 (2017).
[28] D. Dell'Aquila, I. Lombardo, G. Verde, M. Vigilante, L. Acosta, C. Agodi, F. Cappuzzello, D. Carbone, M. Cavallaro, S. Cherubini *et al.*, Phys. Rev. Lett. **119**, 132501 (2017).
[29] K. Kravvaris and A. Volya, Phys. Rev. Lett. **119**, 062501 (2017).
[30] N. Marquardt, W. V. Oertzen, and R. Walter, Phys. Lett. B **35**, 37 (1971).
[31] M. E. Cobern, D. J. Pisano, and P. D. Parker, Phys. Rev. C **14**, 491 (1976).
[32] D. J. Pisano and P. D. Parker, Phys. Rev. C **14**, 475 (1976).
[33] E. Hadjimichael and W. Oelert, *Few-body Problems*, International Review of Nuclear Physics Vol. 3 (World Scientific, Singapore, 1986).
[34] J. Draayer, Nucl. Phys. A **237**, 157 (1975).
[35] Yu. F. Smirnov and Yu. M. Tchuvil'sky, Phys. Rev. C **15**, 84 (1977).
[36] W. Chung, J. van Hienen, B. Wildenthal, and C. Bennett, Phys. Lett. B **79**, 381 (1978).
[37] N. Anantaraman, C. L. Bennett, J. P. Draayer, H. W. Fulbright, H. E. Gove, and J. Tōke, Phys. Rev. Lett. **35**, 1131 (1975).

[38] J. A. Wheeler, Phys. Rev. **52**, 1107 (1937).
[39] K. Wildermuth and E. J. Kanellopoulos, Rep. Prog. Phys. **42**, 1719 (1979).
[40] J. Bang, A. Mazur, A. Shirokov, Y. Smirnov, and S. Zaytsev, Ann. Phys. **280**, 299 (2000).
[41] R. B. Wiringa, S. C. Pieper, J. Carlson, and V. R. Pandharipande, Phys. Rev. C **62**, 014001 (2000).
[42] J.-P. Ebran, E. Khan, T. Nikšić, and D. Vretenar, Nature (London) **487**, 341 (2012).
[43] E. Epelbaum, H. Krebs, D. Lee, and Ulf.-G. Meißner, Phys. Rev. Lett. **106**, 192501 (2011).
[44] S. Elhatisari, D. Lee, G. Rupak, E. Epelbaum, H. Krebs, T. A. Lähde, T. Luu, and U.-G. Meißner, Nature (London) **528**, 111 (2015).
[45] A. C. Dreyfuss, K. D. Launey, T. Dytrych, J. P. Draayer, R. B. Baker, C. M. Deibel, and C. Bahri, Phys. Rev. C **95**, 044312 (2017).
[46] A. Tohsaki, H. Horiuchi, P. Schuck, and G. Röpke, Phys. Rev. Lett. **87**, 192501 (2001).
[47] P. Schuck, Y. Funaki, H. Horiuchi, G. Röpke, A. Tohsaki, and T. Yamada, Phys. Scr. **91**, 123001 (2016).
[48] A. Tohsaki, H. Horiuchi, P. Schuck, and G. Röpke, Rev. Mod. Phys. **89**, 011002 (2017).
[49] A. de Shalit and I. Talmi, *Nuclear Shell Theory*, Pure and Applied Physics Vol. 14 (Academic, New York, 1963).
[50] K. Kravvaris, Ph.D. thesis, The Florida State University, 2018, http://purl.flvc.org/fsu/fd/2018_Su_Kravvaris_fsu_0071E_14611.
[51] K. D. Launey, T. Dytrych, and J. P. Draayer, Prog. Part. Nucl. Phys. **89**, 101 (2016).
[52] A. Volya and Yu. M. Tchuvil'sky, Phys. Rev. C **91**, 044319 (2015).
[53] B. R. Barrett, P. Navrátil, and J. P. Vary, Prog. Part. Nucl. Phys. **69**, 131 (2013).
[54] F. Palumbo and D. Prosperi, Nucl. Phys. A **115**, 296 (1968).
[55] D. Gloeckner and R. Lawson, Phys. Lett. B **53**, 313 (1974).
[56] K. Kravvaris and A. Volya, J. Phys.: Conf. Ser. **863**, 012016 (2017).
[57] M. Moshinsky, *The Harmonic Oscillator in Modern Physics: From Atoms to Quarks*, Documents on Modern Physics (Gordon and Breach, New York, 1969).
[58] L. Trlifaj, Phys. Rev. C **5**, 1534 (1972).
[59] A. Volya and Y. M. Tchuvil'sky, in *Study of Nuclear Clustering Using the Modern Shell Model Approach*, edited by E. Cherepanov, Yu. Penionzhkevich, D. Kamanin, R. Bark, and J. Cornell (World Scientific, Singapore, 2014), p. 215.
[60] R. Wolsky, I. A. Gnilozub, S. D. Kurgalin, and Yu. M. Tchuvil'sky, Phys. At. Nucl. **73**, 1405 (2010).
[61] K. Wildermuth and Y. C. Tang, *A Unified Theory of the Nucleus* (Vieweg, Braunschweig, Germany, 1977).
[62] S. Quaglioni and P. Navrátil, Phys. Rev. C **79**, 044606 (2009).
[63] D. Kurath, Phys. Rev. C **7**, 1390 (1973).
[64] A. Volya and Y. M. Tchuvil'sky, Phys. At. Nucl. **79**, 772 (2016).
[65] Y. M. Tchuvil'sky and A. Volya, JPS Conf. Proc. **6**, 030055 (2015).
[66] D. K. Nauruzbayev, V. Z. Goldberg, A. K. Nurmukhanbetova, M. S. Golovkov, A. Volya, G. V. Rogachev, and R. E. Tribble, Phys. Rev. C **96**, 014322 (2017).
[67] B. A. Brown and W. A. Richter, Phys. Rev. C **74**, 034315 (2006).
[68] T. A. Carey, P. G. Roos, N. S. Chant, A. Nadasen, and H. L. Chen, Phys. Rev. C **23**, 576(R) (1981).
[69] E. S. Diffenderfer, L. T. Baby, D. Santiago-Gonzalez, N. Ahsan, A. Rojas, A. Volya, I. Wiedenhöver, A. H. Wuosmaa, M. P. Carpenter, R. V. F. Janssens *et al.*, Phys. Rev. C **85**, 034311 (2012).
[70] A. M. Long, T. Adachi, M. Beard, G. P. A. Berg, Z. Buthelezi, J. Carter, M. Couder, R. J. deBoer, R. W. Fearick, S. V. Förtsch *et al.*, Phys. Rev. C **95**, 055803 (2017).
[71] A. M. Long, T. Adachi, M. Beard, G. P. A. Berg, M. Couder, R. J. deBoer, M. Dozono, J. Görres, H. Fujita, Y. Fujita *et al.*, Phys. Rev. C **97**, 054613 (2018).
[72] J. Hiura, Y. Abe, S. Saitō, and O. Endō, Prog. Theor. Phys. **42**, 555 (1969).
[73] T. Matsuse and M. Kamimura, Prog. Theor. Phys. **49**, 1765 (1973).
[74] T. Matsuse, M. Kamimura, and Y. Fukushima, Prog. Theor. Phys. **53**, 706 (1975).
[75] R. F. Casten, *Nuclear Structure from a Simple Perspective*, Oxford Studies in Nuclear Physics Vol. 23 (Oxford University Press, Oxford, 2001).
[76] M. Bouhelal, F. Haas, E. Caurier, F. Nowacki, and A. Bouldjedri, Nucl. Phys. A **864**, 113 (2011).
[77] H. W. Fulbright, Annu. Rev. Nucl. Part. Sci. **29**, 161 (1979).
[78] N. Anantaraman, H. Gove, R. Lindgren, J. Tōke, J. Trentelman, J. Draayer, F. Jundt, and G. Guillaume, Nucl. Phys. A **313**, 445 (1979).
[79] R. G. Lovas, R. J. Liotta, A. Insolia, K. Varga, and D. S. Delion, Phys. Rep. **294**, 265 (1998).
[80] J. Okołowicz, M. Płoszajczak, and W. Nazarewicz, Prog. Theor. Phys. Suppl. **196**, 230 (2012).
[81] N. Anantaraman, J. P. Draayer, H. E. Gove, J. Tōke, and H. T. Fortune, Phys. Rev. C **18**, 815 (1978).
[82] M. Ichimura, A. Arima, E. C. Halbert, and T. Terasawa, Nucl. Phys. A **204**, 225 (1973).
[83] F. Tanabe, A. Tohsaki, and R. Tamagaki, Prog. Theor. Phys. **53**, 677 (1975).
[84] Y. Suzuki and K. Hecht, Nucl. Phys. A **455**, 315 (1986).
[85] K. Kravvaris and A. Volya, in *Proceedings of the 4th International Workshop on State of the Art in Nuclear Cluster Physics (SOTANCP4)*, edited by M. Barbui, C. M. Folden III, V. Z. Goldberg, and G. V. Rogachev, AIP Conf. Proc. No. 2038 (AIP, Melville, NY, 2018), p. 020026.
[86] V. Vasilevsky, A. V. Nesterov, F. Arickx, and J. Broeckhove, Phys. Rev. C **63**, 034606 (2001).
[87] V. Vasilevsky, A. V. Nesterov, F. Arickx, and J. Broeckhove, Phys. Rev. C **63**, 034607 (2001).
[88] L. D. Landau and E. M. Lifshitz, *Quantum mechanics. Non-relativistic Theory*, 3rd ed. (Pergamon Press, New York, 1981).
[89] A. I. Baz, I. B. Zeldovich, and A. M. Perelomov, *Scattering, Reactions and Decay in Nonrelativistic Quantum Mechanics (Rasseyanie, Reaktsii i Raspady v Nerelyativistskoi Kvantovoi Mekhanike)* (Israel Program for Scientific Translations, Jerusalem, 1969).
[90] R. G. Thomas, Prog. Theor. Phys. **12**, 253 (1954).
[91] R. Id Betan and W. Nazarewicz, Phys. Rev. C **86**, 034338 (2012).
[92] S. Åberg, P. B. Semmes, and W. Nazarewicz, Phys. Rev. C **56**, 1762 (1997).
[93] R. Bijker and F. Iachello, Ann. Phys. **298**, 334 (2002).

[94] M. Chernykh, H. Feldmeier, T. Neff, P. von Neumann-Cosel, and A. Richter, Phys. Rev. Lett. **98**, 032501 (2007).
[95] A. Volya and V. Zelevinsky, Phys. Rev. C **74**, 064314 (2006).
[96] M. Abramowitz and I. A. Stegun, *Handbook of Mathematical Functions: With Formulas, Graphs, and Mathematical Tables* (Dover, New York, 1965).
[97] A. D. Alhaidari, E. J. Heller, H. A. Yamani, and M. S. Abdelmonem, *The J-matrix Method* (Springer, New York, 2008).
[98] A. M. Shirokov, A. I. Mazur, I. A. Mazur, and J. P. Vary, Phys. Rev. C **94**, 064320 (2016).
[99] H. A. Yamani and L. Fishman, J. Math. Phys. **16**, 410 (1975).
[100] N. Schwierz, I. Wiedenhover, and A. Volya, arXiv:0709.3525 [nucl-th].
[101] A. M. Shirokov, J. P. Vary, A. I. Mazur, and T. A. Weber, Phys. Lett. B **644**, 33 (2007).
[102] G. L. Morgan and R. L. Walter, Phys. Rev. **168**, 1114 (1968).
[103] J. Bond and F. Firk, Nucl. Phys. A **287**, 317 (1977).
[104] T. Stammbach and R. Walter, Nucl. Phys. A **180**, 225 (1972).
[105] S. A. Afzal, A. A. Z. Ahmad, and S. Ali, Rev. Mod. Phys. **41**, 247 (1969).
[106] Yu. F. Smirnov and Yu. M. Tchuvil'sky, Czech. J. Phys. **33**, 1215 (1983).
[107] I. Rotter, Ann. Phys. **471**, 242 (1965).
[108] B. Buck, C. B. Dover, and J. P. Vary, Phys. Rev. C **11**, 1803 (1975).
[109] K. Wildermuth and Y. C. Tang, *A Unified Theory of the Nucleus* (Vieweg, Braunschweig, Germany, 1977), Vol. 1.
[110] M. H. Macfarlane and J. B. French, Rev. Mod. Phys. **32**, 567 (1960).
[111] B. Brown, A. Csótó, and R. Sherr, Nucl. Phys. A **597**, 66 (1996).
[112] Yu. F. Smirnov and D. Chlebowska, Nucl. Phys. **26**, 306 (1961).
[113] O. F. Nemetz, V. G. Neudatchin, A. T. Rudchik, Yu. F. Smirnov, and Yu. M. Tchuvil'sky, *Nucleon Clusters in Atomic Nuclei and Multi-Nucleon Transfer Reactions* (Naukova Dumka, Kiev, 1988), p. 295.
[114] B. A. Brown, Prog. Part. Nucl. Phys. **47**, 517 (2001).
[115] D. Halderson and R. Philpott, Nucl. Phys. A **321**, 295 (1979).
[116] A. Volya, Phys. Rev. C **79**, 044308 (2009).
[117] N. Michel, W. Nazarewicz, M. Płoszajczak, and K. Bennaceur, Phys. Rev. Lett. **89**, 042502 (2002).
[118] P. Descouvemont and M. Dufour, in *Clusters in Nuclei Vol. 2*, edited by C. Beck, Vol. 848 of Lecture Notes in Physics (Springer, Berlin, 2012), p. 1.
[119] T. Fliessbach and H. Mang, Nucl. Phys. A **263**, 75 (1976).
[120] T. Fliessbach and P. Manakos, J. Phys. G **3**, 643 (1977).
[121] S. Saito, Prog. Theor. Phys. **41**, 705 (1969).